Contrib Mineral Petrol (2007) 153:443–463
DOI 10.1007/s00410-006-0159-3

ORIGINAL PAPER

Extreme Sr–Nd–Pb–Hf isotopic compositions exhibited by the Tinaquillo peridotite massif, Northern Venezuela: implications for geodynamic setting

Sung Hi Choi · Samuel B. Mukasa · Alexandre V. Andronikov · Maria C. Marcano

Received: 5 June 2006 / Accepted: 25 October 2006 / Published online: 12 December 2006

Abstract An origin of the Tinaquillo Peridotite Complex in northern Venezuela, and a model for the tectonic framework of the boundary zone between the southern Caribbean Plate margin and the South American Plate (SAP) during Late Jurassic to Mid-Cretaceous time are developed using newly measured Sr, Nd, Pb and Hf isotopic compositions as well as major and trace element geochemistry for some hornblendite veins and their spinel peridotite host rocks. Depleted geochemical characteristics, principally major element concentrations, and Nd and Hf isotopes (e.g., $\varepsilon_{Nd} = +27$; $\varepsilon_{Hf} = +50$; ca. 3.4 Ga-Nd model age) of the Tinaquillo peridotites suggest a genetic link between this complex and the Guiana Shield farther to the south within Venezuela. Scattered zones within the Tinaquillo peridotite were overprinted by what we interpret as channelized hydrous fluids (<~3%) derived from the eastward-dipping subduction of the Farallon Plate beneath the SAP in the Late Jurassic, leading to modification of the original Sr, Nd and Hf isotopic compositions as well as the incompatible element concentrations. The hornblendite veins have Sr, Nd, Pb and Hf isotopic compositions, falling within the range of present-day Pacific/Atlantic MORB, but trace element abundance patterns with combinations of arc- and MORB-like characteristics. These results rule out the possibility of local melting of the host peridotites to produce magmas from which the hornblendite veins formed. We suggest that during inception of the westward-dipping subduction of the Protocaribbean Plate immediately following polarity reversal in the Mid-Cretaceous, melts infiltrated the mantle lithosphere and produced the veins.

Communicated by T.L. Grove.

S. H. Choi · S. B. Mukasa (✉) · A. V. Andronikov · M. C. Marcano
Department Geological Sciences, University of Michigan, 2534 C.C. Little Building, 1100 N. University, Ann Arbor, MI 48109-1005, USA
e-mail: mukasa@umich.edu

Introduction

The tectonized boundary between the southern Caribbean Plate margin and the South American Plate is very broad, locally 500 km in width, and is important to petrology for the exhumed peridotite massifs recording melt depletion, infiltration and channelization processes within mantle domains overprinted by subduction. This region consists of an orogenic belt with several allochthonous oceanic and continental tectonic units piled one on top of the other and dismembered by several brittle and ductile/brittle deformations related to an E–W dextral shear zone with strike-slip faults (e.g., Seyler et al. 1998; Smith et al. 1999; Giunta et al. 2002) (Fig. 1a, b). The Tinaquillo alpine peridotite complex in northern Venezuela is the largest and best mapped of these circum-Caribbean Plate ultramafic massifs (Fig. 1a), and is thought to have been emplaced as a lithospheric fragment during the Late Eocene to Mid-Miocene, by convergence between the North American and South American plates (Ostos et al. 2005). The massif is a layered sub-horizontal, 3-km thick sheet with a mylonitic fabric that parallels compositional layering that seems to have developed well below the peridotite solidus temperature (Seyler and Mattson 1989; Seyler et al. 1998; Giunta et al. 2002;

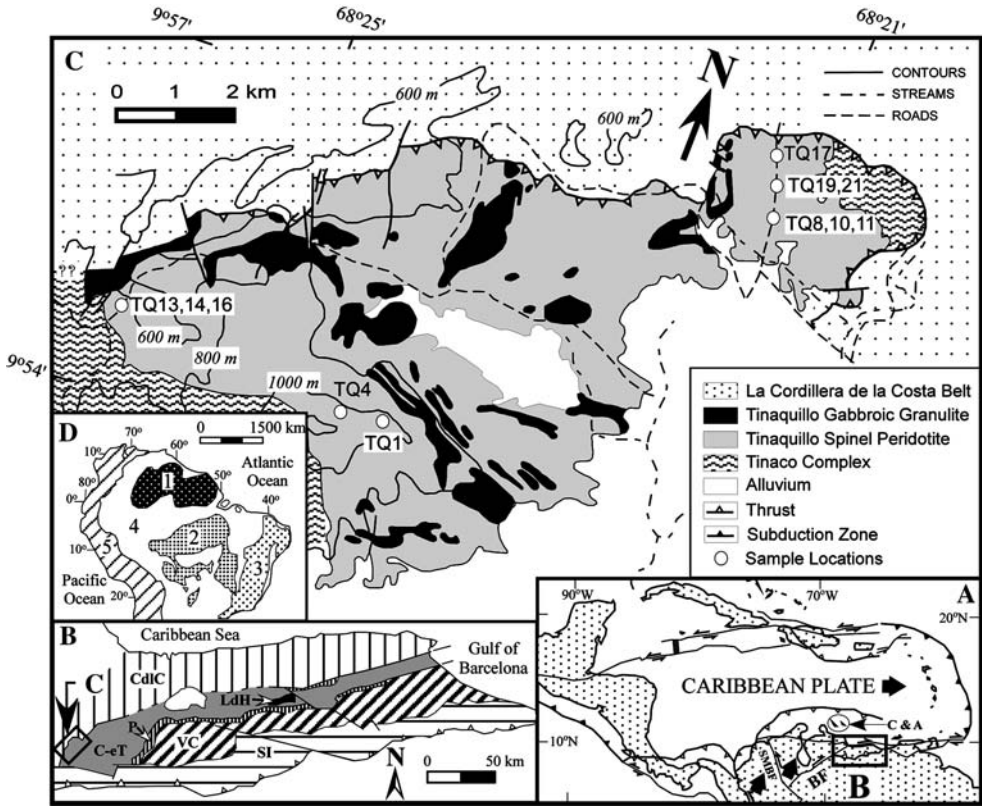

Fig. 1 **a** Schematic geodynamic setting of Caribbean region. Abbreviations are as follows: BF-Boconó fault; C & A-Curaçao and Aruba; SMBF-Santa Marta-Bucaramanga fault. *Thick arrows* are relative motion vectors with respect to South America, after Audemard and Audemard (2002). **b** Generalized tectonic map showing the east–west-trending belts of the western Caribbean Mountain system: *CdlC* Cordillera de la Costa belt; *C-eT* Cacagua-el Tinaco belt; *P* Paracotos belt; *LdH* Loma de Hierro mafic/ultramafic rocks; *VC* Villa de Cura belt; *SI* Serranía del Interior foreland fold and thrust belt. Unlabeled region indicates unmetamorphosed sedimentary cover. This map is after Seyler and Mattson (1989), and Smith et al. (1999). **c** Sample locations on the geologic map of the Tinaquillo peridotite complex in northern Venezuela. The geology is after Seyler and Mattson (1989). **d** Simplified geologic map of South America: *1* Guiana Shield; *2* Central Brazil Shield; *3* Atlantic Shield; *4* Phanerozoic sedimentary cover; *5* Andes, after Teixeira et al. (1989)

Ostos et al. 2005) (Fig. 1c). The complex overlies, and is in thrust contact with, low-grade phyllites of the Cordillera de la Costa belt in the north. It underlies, with an apparently concordant contact, gabbroic to felsic lower continental crustral rocks of the Tinaco complex in the Caucagua-el Tinaco belt to the south and northeast (Seyler and Mattson 1989; Seyler et al. 1998; Giunta et al. 2002; Ostos et al. 2005) (Fig. 1c), potentially providing an important record of mass transfer from the mantle to the crust. However, the nature of the contact with the Tinaco complex, which consists of Paleozoic high-grade metamorphic and igneous rocks (Seyler et al. 1998; Smith et al. 1999; Giunta et al. 2002) is still controversial. MacKenzie (1960) considered it intrusive, Mattson (1985) as a conformably emplaced sheet, and Ostos et al. (2005) as an extensional fault contact zone.

The Tinaquillo complex is composed mainly of spinel peridotites with sills of gabbroic (hornblende) granulites whose layering is defined by hornblende-rich or pyroxene-rich bands that are a few millimeters to centimeters wide (Seyler and Mattson 1989, 1993; Ostos et al. 2005). The peridotites and most of the gabbroic granulites, along with the gneisses of the Tinaco complex that are within ~3 km of the contact with the Tinaquillo complex underwent strong mylonitization at middle amphibolite facies to granulite conditions, with both deformation and recrystallization increasing in intensity toward their mutual tectonic contact (Seyler et al. 1998; Ostos et al. 2005). Timing of the mylonitization is still controversial. Seyler et al. (1998) referred to this intense shearing as the D2 event, and suggested emplacement into the belt during Late Eocene to Mid-Miocene. However, they argued that the mylonitization occurred earlier, at ~90 Ma, based on the Sm–Nd dating of the coeval gabbronoritic sills in the Tinaco complex. Ostos et al. (2005) on the other hand favor a model that calls for NW–SE extension

first followed by NW-directed shear during the Middle to Late Jurassic—as recorded in the deformation structures of the Tinaquillo complex—resulting from alternation in stress regimes during the break-up of Pangea.

Remarkably, the spinel peridotites we sampled are only weakly serpentinized (~1%), and typically have numerous pyroxenite and hornblendite sills and dikes cutting them, although the latter are volumetrically small. Seyler et al. (1998) also reported some plagioclase-hornblendite and felsic sills and dikes, and interpreted them as syn-D1 intrusive products. Well-characterized geochronological data for the Tinaquillo mafic/ultramafic complex itself are non-existent, but Seyler et al. (1998) reported a zircon U–Pb concordia upper intercept age for one of the felsic dikes at 150 ± 2 Ma, taken to represent the time of stabilization of this piece of the lithospheric mantle at the contact with the lower crust.

The association of the Tinaquillo peridotite with sialic crustal rocks, as well as its relative fertility in basaltic components compared to abyssal peridotite, led Seyler and Mattson (1989) and Seyler et al. (1998) to regard this massif as a piece of the sub-continental lithospheric mantle (SCLM), possibly originating beneath the extended continental blocks left between North America and South America by the Jurassic Protocaribbean rifting. However, trace element concentrations of the Tinaquillo gabbroic granulites are transitional between island arc and mid-ocean ridge basalts (MORB) (Seyler and Mattson 1993; Seyler et al. 1998; Ostos and Sisson 2005), suggesting that other tectonic processes besides the Protocaribbean rifting were important. Also, the Caucagua-el Tinaco belt is closely associated with thrusted magmatic terranes showing both arc volcanic rock affinities (the Villa de Cura belt; Fig. 1b) and E- to N-MORB characteristics (the Loma de Hierro unit; Fig. 1b) (e.g., Seyler et al. 1998; Smith et al. 1999; Giunta et al. 2002; Ostos and Sisson 2005). Therefore, Seyler et al. (1998) proposed a model whereby the Tinaquillo massif, starting out as a fragment of continental lithosphere, is modified during back-arc development while positioned between an eastward subducting Farallon Plate and the N–S-spreading Protocaribbean oceanic rift during the Late Jurassic to Mid-Cretaceous. The same authors argued that subduction of the Protocaribbean ridge beneath the arc created the continuous magmatic activity from which the Tinaquillo gabbroic granulite crystallized during that interval. Ostos et al. (2005) on the other hand suggested that the gabbroic melts may have formed entirely by decompressional partial melting of a rising mantle peridotite diapir in a continental rift zone during Pangea break-up with no involvement of subduction at all, and that the residual material of the event might be the Tinaquillo peridotites. Magmas produced during these scenarios should have isotopic and trace element characteristics that are easily distinguished from each other, and therefore the study reported here was designed to identify the appropriate tectonic model.

We have determined the Sr, Nd, Pb and Hf isotopic compositions as well as major and trace element compositions of the Tinaquillo spinel peridotite and hornblendite veins with the aim of documenting the isotopic and trace element signatures of the components in the massif, estimating their spatial distribution, and placing them in the most plausible tectonic setting at the time of their development. The data unequivocally support a SCLM origin for the Tinaquillo peridotite, and rule out origination of the hornblendite veins by decompressional melting of the host peridotite. On the basis of the chemical relationships between the peridotite and its veins and dikes, we propose a new tectonic framework for understanding the defuse boundary between the southern margin of the Caribbean Plate and the South American Plate.

Samples and analytical procedures

Tinaquillo peridotites overall exhibit a porphyroclastic texture, and consist of olivine and enstatite megaporphyroclasts (5–10 mm), commonly strained, with smaller porphyroclasts (~1 mm) of olivine, enstatite, diopside and brown spinel, set in a fine-grained (<0.2 mm) matrix of the four phases. Porphyroclastic enstatite contains clinopyroxene exsolution lamellae, but clinopyroxene grains also occur with enstatite lamellae. The grains in the matrix are mostly tabular, defining a strong to moderate fabric, and are free of exsolution lamellae.

Tinaquillo hornblendite veins (from 2 cm thick for TQ-19 to 7 cm for TQ-14) exhibit a continuum of textures from porphyroclastic to equigranular, and in addition to the 0.2-mm to 1.5-cm amphibole, contain small amount of other minerals (up to 0.5 mm), chiefly orthopyroxene, olivine, green spinel and magnetite. They have no fabrics, but kink bands in amphibole and orthopyroxene are common. The amphiboles in the Tinaquillo hydrous veins usually have oriented inclusions of clinopyroxene and orthopyroxene which at first seem to be exsolution lamellae. However, in backscattered electron images, no halos due to compositional gradients around the inclusions are observed. We have therefore interpreted the pyroxene

Table 1 Major and trace element concentrations for Tinaquillo Peridotite Complex, northern Venezuela

Sample	TQ-01	TQ-04	TQ-10	TQ-11	TQ-13	TQ-16	TQ-17	TQ-08	TQ-19	TQ-21
Rock type	Sp. perid.	Sp. perid.	Sp. perid.	Sp. perid.	Sp. perid.	Sp. perid.	Sp. perid.	Hornblendite	Hornblendite	Hornblendite
SiO_2	43.8	43.6	42.4	44.8	41.3	43.0	42.5	42.8	41.5	43.0
TiO_2	0.07	0.04	0.07	0.07	0.06	0.08	0.08	1.91	1.12	1.27
Al_2O_3	2.9	2.1	2.4	3.2	1.9	2.9	3.1	15.4	16.4	15.0
Fe_2O_3*	8.3	8.9	8.6	8.4	8.7	8.3	8.9	5.9	7.7	6.3
MnO	0.13	0.13	0.12	0.13	0.12	0.12	0.13	0.08	0.10	0.08
MgO	41.1	42.9	42.0	40.6	42.7	41.2	41.6	19.2	17.8	18.5
CaO	2.7	2.0	2.3	2.7	1.7	2.8	2.6	9.9	11.6	11.3
Na_2O	0.23	ND	0.23	1.10	0.88	0.26	0.20	2.60	2.34	2.86
K_2O	ND	ND	ND	ND	ND	ND	ND	0.19	0.09	0.20
P_2O_5	ND	0.01	ND	ND	0.01	ND	ND	0.02	ND	0.03
Total	99.2	99.6	98.1	101.1	97.4	98.6	99.1	98.0	98.7	98.5
Mg#**	90.7	90.5	90.7	90.5	90.6	90.7	90.3	86.7	82.1	85.4
V	119	55	59	66	45	66	66	323	523	421
Cr	4116	2779	2638	2663	2386	2816	2765	467	215	ND
Sr	ND	3.21	4.68	2.23	2.18	3.38	2.46	205.54	94.61	434.00
Y	ND	1.38	2.16	2.90	1.48	2.57	2.59	22.63	16.31	16.51
Nb	ND	0.12	0.20	0.05	0.11	0.05	0.15	ND	0.11	1.01
Hf	ND	0.08	0.13	0.11	0.09	0.15	0.11	1.03	0.44	1.09
Ta	ND	0.02	0.02	0.01	0.01	0.01	0.01	0.14	0.01	0.07
Pb	ND	0.21	0.22	0.09	0.14	0.06	0.16	0.02	ND	0.65
Th	ND	0.02	0.02	0.01	0.02	0.02	0.01	0.02	0.03	0.24
U	ND	0.04	0.04	0.02	0.01	0.22	0.02	ND	0.03	0.07
Ba	ND	3.17	3.98	5.17	3.86	5.04	6.12	22.40	9.74	29.41
La	ND	0.10	0.08	0.03	0.03	0.03	0.04	0.86	0.11	4.37
Ce	ND	0.27	0.26	0.10	0.12	0.20	0.11	4.65	1.03	12.53
Pr	ND	0.04	0.06	0.03	0.04	0.06	0.04	0.88	0.24	1.95
Nd	ND	0.19	0.29	0.19	0.20	0.34	0.24	5.55	1.87	9.09
Sm	ND	0.13	0.16	0.13	0.13	0.18	0.16	2.26	1.11	2.24
Eu	ND	0.03	0.07	0.06	0.05	0.07	0.07	0.97	0.48	0.82
Gd	ND	0.11	0.24	0.24	0.15	0.25	0.23	3.06	1.77	2.45
Tb	ND	0.03	0.04	0.05	0.03	0.05	0.05	0.58	0.37	0.42
Dy	ND	0.21	0.35	0.43	0.22	0.40	0.39	3.84	2.55	2.66
Ho	ND	0.05	0.09	0.11	0.06	0.10	0.10	0.82	0.60	0.55
Er	ND	0.16	0.27	0.32	0.16	0.28	0.29	2.28	1.61	1.62
Yb	ND	0.14	0.20	0.33	0.13	0.29	0.27	1.97	1.37	1.36
Lu	ND	0.03	0.03	0.06	0.02	0.04	0.05	0.29	0.20	0.20
$(La/Yb)_N$***	–	0.55	0.28	0.06	0.15	0.09	0.10	0.31	0.06	2.30

Values are wt% for major elements, and ppm for trace elements

ND not determined

*Total Fe as Fe_2O_3

** 100 Mg/(Mg + ΣFe)

*** Normalized to the composition of chondritic meteorites (Sun and McDonough 1989)

Table 2 Rb–Sr, Sm–Nd, and Pb isotopic compositions for Tinaquillo Peridotite Complex, northern Venezuela

Sample no	[Rb] ppm	[Sr] ppm	$^{87}Rb/^{86}Sr$	$^{87}Sr/^{86}Sr \pm 2\sigma$	[Sm] ppm	[Nd] ppm	$^{147}Sm/^{144}Nd$[a]	$^{143}Nd/^{144}Nd \pm 2\sigma$	ε_{Nd}	T_{DM} (Ma)	$^{206}Pb/^{204}Pb$	$^{207}Pb/^{204}Pb$	$^{208}Pb/^{204}Pb$
Spinel peridotites													
TQ-01 wr	0.018	0.95	0.0535	–	0.08	0.17	0.2937	0.513566 ± 26	18.1	847	19.01	15.58	38.23
cpx (*c*)	–	–	–	0.70577 ± 32	–	–	–	0.513588 ± 27	18.5	–	–	–	–
cpx (*d*)	–	–	–	0.70666 ± 89	–	–	–	0.513615 ± 50	19.1	–	–	–	–
TQ-04 wr	0.044	–	–	0.70277 ± 4	0.06	0.29	0.1254	0.513095 ± 24	8.9	33	19.24	15.64	38.55
TQ-10 wr	0.026	5.29	0.0143	0.70292 ± 2	0.18	0.40	0.2697	0.513236 ± 30	11.7	325	18.71	15.57	38.11
TQ-11 wr	0.007	2.37	0.0087	0.70357 ± 9	0.12	0.28	0.2516	0.513994 ± 33	26.5	3,396	18.69	15.55	38.11
duplicate	–	–	–	–	–	–	–	–	–	–	18.71	15.60	38.21
cpx (*c*)	–	–	–	0.70221 ± 2	–	–	–	0.513977 ± 20	26.1	–	18.34	15.59	38.21
TQ-13 wr	0.098	–	–	0.70353 ± 11	0.94	0.33	0.1698	0.513317 ± 22	13.3	–731	18.39	15.54	37.80
cpx (*c*)	–	–	–	0.70343 ± 12	–	–	–	–	–	–	–	–	–
TQ-16 wr	0.017	–	–	0.70355 ± 9	0.22	0.43	0.3053	0.513275 ± 18	17.1	265	18.06	15.49	37.50
TQ-17 wr	0.071	–	–	0.70338 ± 9	0.14	0.35	0.2351	0.513515 ± 22	12.4	2,673	18.63	15.59	38.17
Hornblendite veins													
TQ-08 wr	0.683	225.32	0.0088	0.70231 ± 14	2.44	6.10	0.2424	0.513112 ± 15	9.3	–10	18.42	15.52	37.84
TQ-14 amp	–	–	–	0.70263 ± 2	1.33	2.63	0.3064	0.513222 ± 20	11.4	176	18.36	15.53	37.97
TQ-19 wr	0.570	–	–	0.70256 ± 5	1.08	2.00	0.3286	0.513289 ± 16	12.7	230	18.53	15.55	37.98
TQ-21 wr	0.655	484.88	0.0039	0.70253 ± 2	2.41	9.93	0.1469	0.513052 ± 21	8.1	145	18.32	15.46	37.78
amp	–	–	–	0.70251 ± 1	2.59	10.89	0.1440	0.513053 ± 18	8.1	136	18.32	15.52	37.94

ε_{Nd} is calculated with $(^{143}Nd/^{144}Nd)_{CHUR} = 0.512638$. T_{DM} is calculated with the DM parameters of $^{147}Sm/^{144}Nd = 0.2124$ and $^{143}Nd/^{144}Nd = 0.513114$

c clean separates, *d* dirty separates, *wr* whole-rock, *cpx* clinopyroxene, *amp* amphibole

[a] Uncertainty is ~0.5%

inclusions to be the result of epitaxial overgrowth on pargasitic amphibole. The absence of strong serpentinization and the lack of equilibration in the plagioclase peridotite stability field suggest a relatively rapid ascent of the ultramafic body through the upper mantle and crust.

Seven spinel peridotites and four hornblendite veins have been analyzed for major and trace element concentrations (Table 1), and Sr, Nd, Pb and Hf isotopic compositions (Tables 2, 3). The spinel peridotites studied have been sampled far from the mafic veins, and the veins by taking the medial materials away from the contacts. Whole-rock powders and clinopyroxene and amphibole separates were prepared from samples free of any visible surface weathering following established procedures summarized by Mukasa and Shervais (1999). The spinel peridotites are affected by less than 1% serpentinization.

Major elements were analyzed by X-ray fluorescence (XRF) spectrometry at Michigan State University, following procedures described in Hannah et al. (2002). Standards (JB-1a-1, JB-1a-5 and W-2) were analyzed with the unknown samples, and reported in Choi et al. (2006). The data were reduced by weighted regression using compiled analyses on the standard materials. Trace elements were analyzed by inductively-coupled-plasma mass spectrometry (ICP-MS) at the same laboratories. Precision was estimated to be within 5% for the XRF and 10% for the ICP-MS from replicate analyses of the standards.

The Sr, Nd and Pb isotope analyses, including chemical separation and running on VG Sector thermal ionization mass spectrometers, were performed at the University of Michigan. Details of the analytical procedures appear in Mukasa et al. (1991). Sample dissolutions were carried out in concentrated HF and HNO_3 (10:1) on a hot plate. Owing to the low abundance of Sr in the samples studied, we dissolved ~200–500 mg of whole-rock powder for the Sr separations; generally smaller amounts of sample (~150–300 mg) were used for the Sm, Nd, Pb, Lu and Hf separations. Typical sample weights for the mineral separates were ~90 mg. Samarium, Nd, Sr and Rb concentrations were measured by isotope dilution with enriched ^{149}Sm, ^{150}Nd, ^{84}Sr and ^{87}Rb spikes. Pb concentrations were measured by ICP-MS. $^{87}Sr/^{86}Sr$ and $^{143}Nd/^{144}Nd$ ratios were corrected for instrumental mass fractionation by normalizing to $^{86}Sr/^{88}Sr = 0.1194$ and $^{146}Nd/^{144}Nd = 0.7219$, respectively. Replicate analyses of NBS-987 and La Jolla standards gave $^{87}Sr/^{86}Sr = 0.710255 \pm 11$ ($N = 30$, $2\sigma_m$) and $^{143}Nd/^{144}Nd = 0.511848 \pm 19$ ($N = 30$, $2\sigma_m$), respectively. Measured Pb isotopic ratios were corrected for instrumental mass fractionation of 0.1% per atomic mass unit by references to replicate analyses of the standard NBS-981. Total blanks averaged 0.2 ng for Sr, 0.04 ng for Nd, and 0.02 ng for Pb.

Table 3 Lu-Hf isotopic compositions for Tinaquillo Peridotite Complex, northern Venezuela

Sample no	[Lu] ppm	[Hf] ppm	$^{176}Lu/^{177}Hf$	$^{176}Hf/^{177}Hf$	2σ	ε_{Hf}
Spinel peridotites						
TQ-01 wr	0.045	0.044	0.1464	–	–	–
TQ-04 wr	0.029	0.051	0.0806	0.283849	0.000147	38
Duplicate	–	–	–	0.283842	0.000440	38
TQ-10 wr	0.040	0.100	0.0633	0.283041	0.000099	10
TQ-11 wr	0.057	0.112	0.0810	0.284187	0.000069	50
Duplicate	–	–	–	0.283942	0.000400	41
TQ-11 cpx	0.283	0.654	0.0613	0.284141	0.000028	48
TQ-13 wr	0.028	0.075	0.0588	0.283717	0.000158	33
TQ-16 wr	0.046	0.121	0.0606	0.283306	0.000232	19
Duplicate	–	–	–	0.283036	0.000237	9
Triplicate	–	–	–	0.283282	0.000318	18
TQ-17 wr	0.046	0.094	0.0786	0.284053	0.000191	45
Hornblendite veins						
TQ-08 wr	0.329	1.489	0.0352	0.282990	0.000013	8
TQ-14 amp	0.244	0.637	0.0543	0.283453	0.000019	24
TQ-19 wr	0.222	0.614	0.0575	0.283117	0.000074	12
TQ-21 wr	0.218	1.233	0.0251	0.283192	0.000018	15
TQ-21 amp	0.198	1.345	0.0209	0.283167	0.000040	14

ε_{Hf} is calculated with $^{176}Hf/^{177}Hf = 0.282772$ for present-day chondritic Earth

Error for [Hf], [Lu] and $^{176}Lu/^{177}Hf$ are ~2% (2σ)

wr whole-rock, *cpx* clinopyroxene, *amp* amphibole

The Hf isotope analyses were determined with the multiple-collector ICP-MS (Nu-Plasma HR) at the University of Michigan, following column separation procedures summarized by Münker et al. (2001). Lu and Hf concentrations were measured by isotope dilution with enriched ^{176}Lu and ^{178}Hf spikes, respectively. To monitor machine performance, we analyzed the JMC-475 Hf standard after every three samples, obtaining a ^{176}Hf/^{177}Hf value of 0.282120 ± 25 (N = 26, $2\sigma_m$). Values reported for the samples are therefore adjusted to correspond to the accepted value of 0.282160 for the JMC-475 Hf standard. The total procedural blank level was about 0.02 ng for Hf.

Results and interpretations

Major element compositions

The whole-rock *mg-numbers* (100Mg/(Mg + ΣFe)) of the Tinaquillo spinel peridotites have a range from 90.3 to 90.7 (Table 1). Variations in major oxide concentrations as a function of MgO, good indicators of the refractoriness of the peridotites, are shown in Fig. 2. The Tinaquillo peridotites are depleted in basaltic components, such as Al_2O_3, CaO and TiO_2, relative to the primitive mantle (Fig. 2). The abundances and trends illustrated in Fig. 2 are compatible with the best-fit lines for world-wide spinel peridotite xenolith compositions, suggesting an origin as a residue left after basaltic melt extraction.

The Tinaquillo hornblendite veins have relatively high Na_2O (2–3 wt%) and TiO_2 (1–2 wt%) concentrations, and low *mg-numbers* (82–87) relative to the peridotites (Table 1). However, this range in *mg-numbers* is too high for melts derived from a primitive lherzolite, and is more consistent with an origin as high-pressure cumulates from mafic melts or as reaction products in interactions between basaltic melts and the host peridotite, as first suggested in studies of alpine peridotites and composite mantle-derived xenoliths (e.g., Bodinier et al. 1988, 1990; Mukasa and Shervais 1999).

Trace element compositions

Tinaquillo peridotite $(Yb)_N$ values, normalized to chondrite, are variable from 0.8 to 1.9 (Table 1; Fig. 3a, b). Abundance of the heavy rare earth elements (HREE) in the peridotites, such as Yb, has a negative correlation with MgO concentrations (Table 1). The peridotites show light rare earth element (LREE) depleted patterns (Table 1; Fig. 4a), most likely the result of basaltic melt extraction from a primitive mantle (i.e., the same process that controls the major element trends). The extended primitive mantle-normalized trace element patterns of the peridotites shown overall on the element distribution diagram in Fig. 4a reveal depletion in the highly incompatible elements relative to less incompatible ones. This supports the interpretation of melt extraction being the dominant process to have affected the peridotites. Superimposed on this primary signature is the secondary signature of enrichments in Ba, U over Th, and Pb over neighboring REE, interpreted to represent addition of a subduction component by fluid activity. However, these peridotites do not show depletion in Nb relative to La.

The hornblendite veins have high REE concentrations, $(Yb)_N$ = 8.0 – 11.6, relative to the peridotites, and two types of REE patterns: LREE-enriched (TQ-8 and TQ-21) and LREE-depleted (TQ-19) (Table 1; Fig. 4b). Downes (2001) reported that LREE-enriched hornblendites are fairly common in amphibole-rich veins in peridotites at other localities worldwide. Eu anomalies are not observed, indicating that at no time was plagioclase a fractionating phase. This means that the veins formed at mantle pressures, not during exhumation through the crust. The hornblendites show strong Nb negative and Sr positive anomalies relative to the neighboring elements on the element distribution diagram (Fig. 4b). In addition, they are depleted in HREE relative to N-MORB. These are features indicative of an island arc affinity. However, the most incompatible large ion lithophile elements (LILE), such as Rb, Ba, Th and U, in the hornblendites are depleted relative to LREEs, and have low concentrations compared to typical arc basalt.

Sr–Nd–Pb–Hf isotopic compositions

The Sr, Nd and Pb isotopic compositions for whole-rock and clinopyroxene separates from the Tinaquillo peridotites are listed in Table 2. It was difficult to obtain high-precision Sr isotopic data for these peridotites because of the exceedingly low Sr concentrations (2–5 ppm; Table 1). We analyzed two carefully hand-picked, ultra-clean clinopyroxene separates with the whole-rock samples for TQ-11 and TQ-13 to assess the significance of secondary alteration. For sample TQ-13, Sr isotopic ratios for the whole-rock and its clinopyroxene separate are indistinguishable within our cited analytical uncertainties, whereas for TQ-11 the clinopyroxene is significantly more unradiogenic compared to its whole-rock (^{87}Sr/^{86}Sr = 0.70221 and 0.70357, respectively, Table 2). However, the Nd isotopic ratios of the whole-rock and clinopyroxene separate from

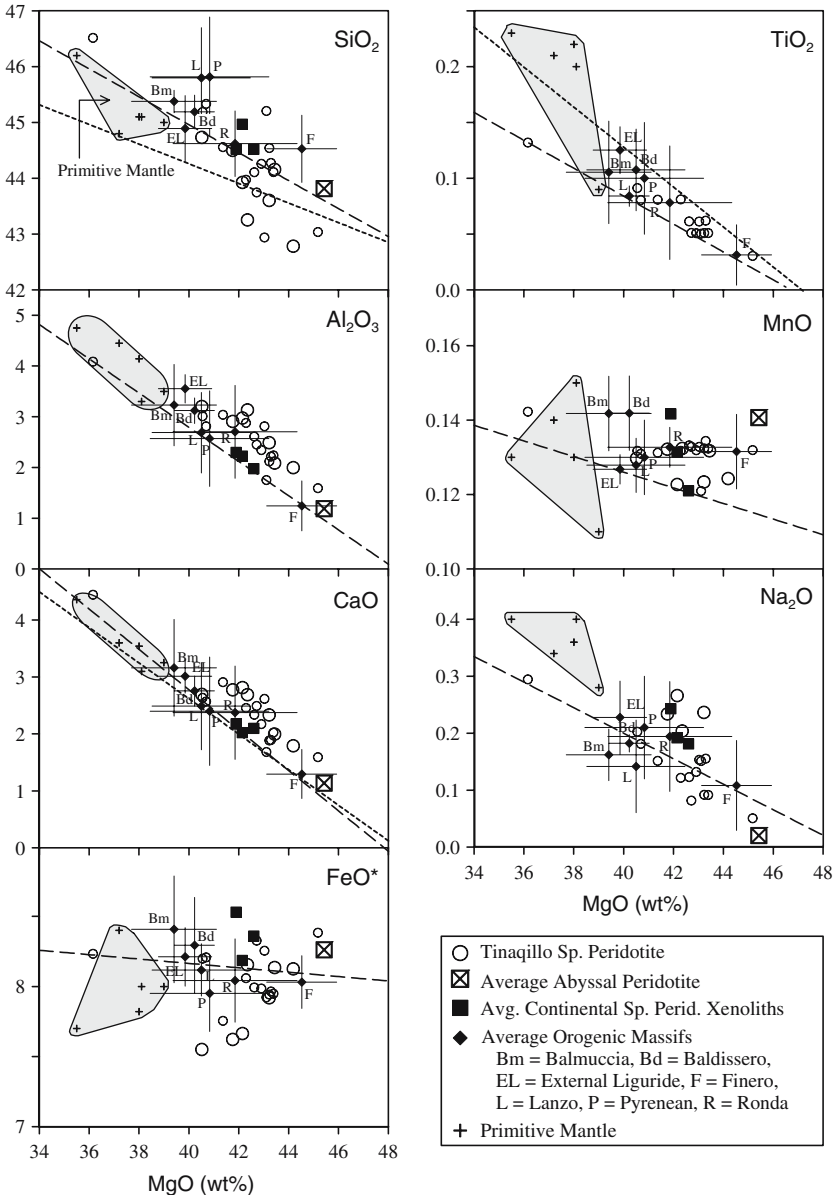

Fig. 2 Variation diagrams for whole-rock major oxides (wt%) versus whole-rock MgO concentrations for the Tinaquillo spinel peridotites. The *dashed lines* are the best-fit lines for spinel lherzolite xenoliths elsewhere from Maalϕe and Aoki (1977), and the dotted lines are from McDonough (1990). Data for the Tinaquillo peridotites (*small circles*) are from Seyler and Mattson (1989). The *diamond* and *cross* represent the average composition and one standard error of the Alpine orogenic peridotite massif. Data sources: primitive mantle (Hutchison 1974; Ringwood 1979; Wänke 1981; Palme and Nickel 1985; McDonough 1990), average continental spinel peridotites (Maalϕe and Aoki 1977; Hartmann and Wedepohl 1990; McDonough 1990), average abyssal peridotite (Boyd 1989), and orogenic massifs; Baldissero (n = 14, Hartmann and Wedepohl 1993), Balmuccia (n = 29, Hartmann and Wedepohl 1993; Mukasa and Shervais 1999), External Liguride (n = 20, Rampone et al. 1995), Finero (n = 11, Hartmann and Wedepohl 1993), Lanzo (n = 12, Bodinier 1988), Pyrenean (n = 31, Bodinier et al. 1988), Ronda (n = 14, Frey et al., 1985)

sample TQ-11 are indistinguishable within the reported analytical uncertainties (Table 2). The same is true for the $^{207}Pb/^{204}Pb$ and $^{208}Pb/^{204}Pb$ values, but variability is noted in the $^{206}Pb/^{204}Pb$ ratios (Table 2). To test for reproducibility, we ran the whole-rock sample in duplicate, but did not have enough clinopyroxene separate to do the same for this mineral. The whole-rock Pb isotopic compositions were reproduced within uncertainty. Therefore, we interpret the ~2% discrepancy in $^{206}Pb/^{204}Pb$ ratios between whole-rock and clinopyroxene as either the result of analytical error or alteration of the peridotite while clinopyroxene remained pristine. For further verification of data quality, we analyzed an ultra-clean clinopyroxene separate from sample TQ-1 to compare it with the data for a ''dirty'' clinopyroxene separate for which some of the grains were composites. Their isotopic ratios do not show appreciable differences, and in fact can be considered good duplicates. The Hf isotopic compositions are listed in Table 3. Due to the low Hf concentration in the Tinaquillo peridotites (0.04–0.12 ppm), we have run the samples in duplicate or triplicate to verify reproducibility, which is demonstrated within the cited uncertainties. For one sample (TQ-11), a whole-rock and clinopyroxene separate have both been analyzed for their Hf isotopic compositions, in this case as well obtaining good agreement within the uncertainties (Table 3).

Peridotites in the Tinaquillo Complex have the following isotopic compositions: $^{87}Sr/^{86}Sr$ = 0.70221 – 0.70666, $^{143}Nd/^{144}Nd$ = 0.513095 – 0.513994 (ε_{Nd} = +9

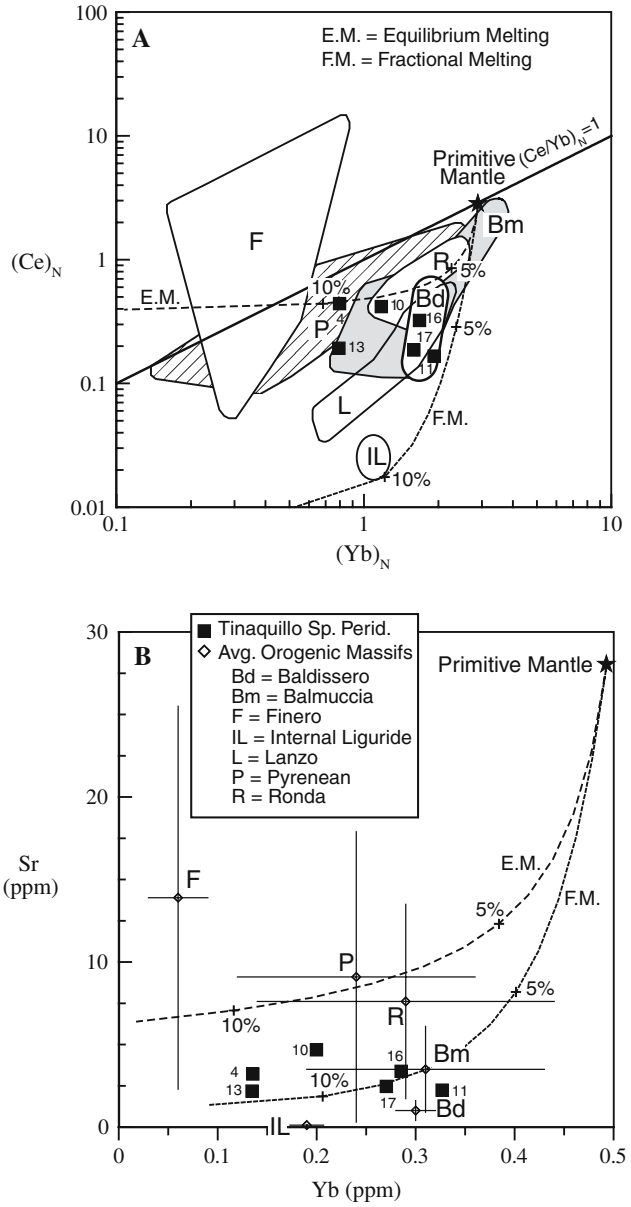

Fig. 3 **a** $(Ce)_N$ versus $(Yb)_N$ ratios, and **b** Sr versus Yb concentrations (ppm), for the Tinaquillo spinel peridotites normalized to the CHUR values (Sun and McDonough 1989). The *diamond* and *cross* represent the average composition and one standard error of the available data on Alpine orogenic peridotite massifs. Data for the Internal Liguride are from Rampone et al. (1996), and for the others as in Fig. 2. The dashed lines indicate residual trends for the non-modal equilibrium melting (*EM*) and the fractional melting (*FM*) of garnet peridotite with primitive mantle compositions (Jagoutz et al. 1979; Sun and McDonough 1989). The source mineralogy and melting phase proportions were taken from Takazawa et al. (2000). Partition coefficients are from Kennedy et al. (1993), Hauri et al. (1994), and Takazawa et al. (2000)

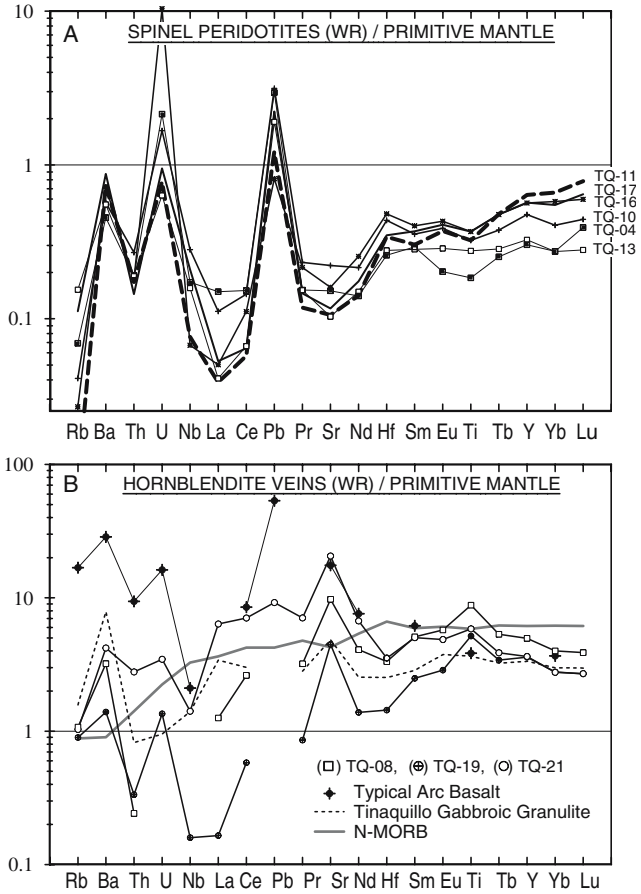

Fig. 4 Whole-rock trace element abundances for the Tinaquillo spinel peridotites and hornblendite veins, normalized to primitive mantle values (Sun and McDonough 1989). Tinaquillo gabbroic granulite (Giunta et al. 2002), typical arc basalt (McCulloch and Gamble 1991), and N-MORB (Sun and McDonough 1989) are also shown for comparison

to +27), $^{206}Pb/^{204}Pb$ = 18.06 – 19.24, $^{207}Pb/^{204}Pb$ = 15.49 – 15.64, $^{208}Pb/^{204}Pb$ = 37.50 – 38.55, and $^{176}Hf/^{177}Hf$ = 0.283036 – 0.284187 (ε_{Hf} = +9 to +50) (Tables 2, 3). Sr–Nd, Nd–Hf, and Pb–Pb isotopic correlation diagrams are shown in Fig. 5a–d. For comparison, the hypothetical mantle reservoirs of DMM, HIMU, EM1 and EM2 (DMM = depleted mantle, EM1 and EM2 = enriched mantle type 1 and 2, HIMU = mantle with high U/Pb ratio; Zindler and Hart 1986) and the fields for MORB are also shown on these diagrams. The Pb isotopic signatures show ranges that overlap with present-day Pacific and Atlantic MORB, falling on or close to the northern hemisphere regression line (NHRL) of Hart (1984) (Fig. 5c, d). The $^{143}Nd/^{144}Nd$ and $^{176}Hf/^{177}Hf$ ratios (Fig. 5b), overlap with MORB, but extend to more depleted compositions (i.e., high $^{143}Nd/^{144}Nd$ and $^{176}Hf/^{177}Hf$ ratios), resulting from the time-integrated effect of basaltic melt extractions leaving an incompatible-element-depleted residue. It is remarkable that sample TQ-11 exhibits strongly depleted Nd and Hf isotopic compositions (ε_{Nd} = +27;

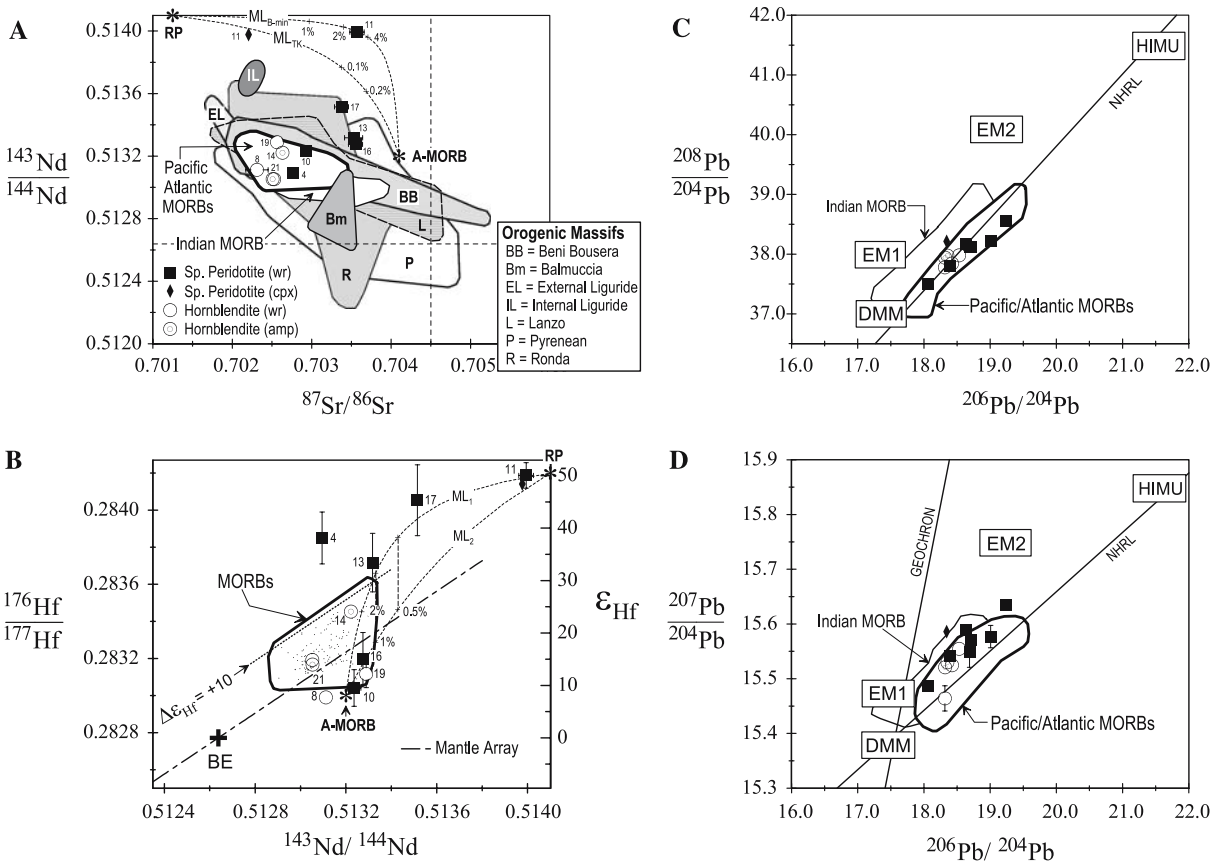

Fig. 5 **a** $^{143}Nd/^{144}Nd$ versus $^{87}Sr/^{86}Sr$, **b** $^{176}Hf/^{177}Hf$ versus $^{143}Nd/^{144}Nd$, **c** $^{208}Pb/^{204}Pb$ versus $^{206}Pb/^{204}Pb$, and **d** $^{207}Pb/^{204}Pb$ versus $^{206}Pb/^{204}Pb$ isotopic ratios for the Tinaquillo peridotites and hornblendite veins. For comparison, Sr and Nd isotopic compositions of clinopyroxene separated from the peridotite massifs of Ronda (Reisberg and Zindler 1986; Reisberg et al. 1989), Pyrenean (Downes et al. 1991; Mukasa et al. 1991), Beni Bousera (Pearson et al. 1993), Balmuccia (Mukasa and Shervais 1999), Lanzo (Bodinier et al. 1991), External Liguride (Rampone et al. 1995), and Internal Liguride (Rampone et al. 1996) are also shown. Mantle components and fields for oceanic basalts are from Zindler and Hart (1986), and Chauvel and Blichert-Toft (2001). The $^{176}Hf/^{177}Hf$ value of bulk Earth (*BE*) and the Mantle array in (**b**) are from Blichert-Toft and Albarède (1997) and Blichert-Toft et al. (1999). The data set for N-MORB is from Salters (1996), Salters and White (1998), Chauvel and Blichert-Toft (2001), Andres et al. (2004), Hanan et al. (2004) and Blichert-Toft et al. (2005). The reference line of $\Delta\varepsilon_{Hf} = +10$ is shown for comparison in (**b**), where $\Delta\varepsilon_{Hf} = \varepsilon_{Hf} - (1.36\varepsilon_{Nd} + 3.0$; Vervoort and Blichert-Toft 1999), after the notation of Beard and Johnson (1993). NHRL is the Northern Hemisphere Reference Line from Hart (1984). Error bars are 2σ uncertainties, and are given only where they exceed the size of the symbol in the plot. *ML* mixing line; *RP* residual peridotite protolith; *MORB* mid-ocean ridge basalts; *A-MORB* altered-MORB; *EM1* and *EM2* enriched mantle type 1 and 2, respectively; *HIMU* mantle with high U/Pb ratio. See the text in detail

$\varepsilon_{Hf} = +50$), in marked contrast to the present-day MORB source mantle. These results are supported by the ε_{Nd} value (+26; Table 2) and the ε_{Hf} value (+48; Table 3) of its constituent clinopyroxene. In Fig. 5b, we have shown the Nd–Hf 'mantle array' proposed by Vervoort and Blichert-Toft (1999). Deviation from the mantle array can be denoted using the $\Delta\varepsilon_{Hf}$ notation of Beard and Johnson (1993), where $\Delta\varepsilon_{Hf} = \varepsilon_{Hf} - (1.36\ \varepsilon_{Nd} + 3.0)$ (Vervoort and Blichert-Toft 1999). The value of $\Delta\varepsilon_{Hf}$ for sample TQ-11 is ~+8, which suggests robust coupling of the Hf and Nd isotopic compositions in the sample, considering that MORB data by contrast exhibit wide variations ($\varepsilon_{Hf} = +11 - +29$; Fig. 5b). The unusually radiogenic Sr for some samples (clinopyroxene separates as well whole-rocks), falling off the Sr–Nd mantle array, appears to be the result of infiltration by subduction-derived fluids at some stage in the massif's history, but not during any seafloor or subaerial alteration as this is not a universal feature for all rocks in the massif.

The Tinaquillo hornblendite veins have a limited range in Sr, Nd, Pb and Hf isotopic compositions: $^{87}Sr/^{86}Sr = 0.70231 - 0.70263$, $^{143}Nd/^{144}Nd = 0.513052 - 0.513289$ ($\varepsilon_{Nd} = +8$ to $+13$), $^{206}Pb/^{204}Pb = 18.32 - 18.53$, $^{207}Pb/^{204}Pb = 15.46 - 15.55$, $^{208}Pb/^{204}Pb = 37.78 - 37.98$, and $^{176}Hf/^{177}Hf = 0.282990 - 0.283453$ ($\varepsilon_{Hf} = +8$ to

+24) (Tables 2, 3), falling within the Atlantic and Pacific MORB fields on all of the isotopic correlation diagrams, Sr–Nd (Fig. 5a), Nd–Hf (Fig. 5b), and Pb–Pb (Fig. 5c, d). This is markedly different compared to the host peridotites which have a wide range in Nd and Hf isotopic compositions—from MORB-like to strongly depleted than MORB, and even having highly radiogenic Sr that places some samples to the right of the mantle array. For sample TQ-21, both whole-rock and amphibole separates have been analyzed and these yield indistinguishable results (Tables 2, 3).

Discussion

Tinaquillo peridotite origination in the sub-continental lithospheric mantle (SCLM)

Previous studies (e.g., Boyd 1989; Johnson et al. 1990; Griffin et al. 1999; Bizimis et al. 2000; Downes 2001) have suggested that the lithospheric mantle composition is related to the tectonic setting in which stabilization occurred and to time since that event. That is to say, (1) abyssal peridotites, recognized to be residues of the mantle melting that forms MORB, have undergone repeated decompression partial melting; (2) supra-subduction zone (SSZ) peridotites are characterized by significantly more depletion compared to abyssal peridotites, achieved during the flux melting of a depleted-MORB source mantle and subsequent re-enrichment in LREE and other incompatible elements as a result of metasomatism by subduction zone fluids; and (3) mean SCLM compositions have evolved from the hypothesized highly depleted Archean mantle to more fertile mantle during Phanerozoic times as the result of metasomatism and melt infiltration.

In order to understand which among these factors were important in the development of the Tinaquillo peridotite, we have compared available major oxide compositions for the average abyssal peridotite and European alpine-type orogenic peridotites to our new data, and these are illustrated in Figs. 2 and 6. In addition, the mean SCLM compositions of archons, protons and tectons, as defined by Griffin et al. (1999), (i.e., lithospheric mantle that experienced its last tectonothermal event at >2.5 Ga, 2.5–1.0 Ga and <1.0 Ga, respectively, inferred from the age of the overlying crust), are also shown for comparison in Fig. 6. The Tinaquillo peridotites are generally more depleted in the basaltic components relative to the better known

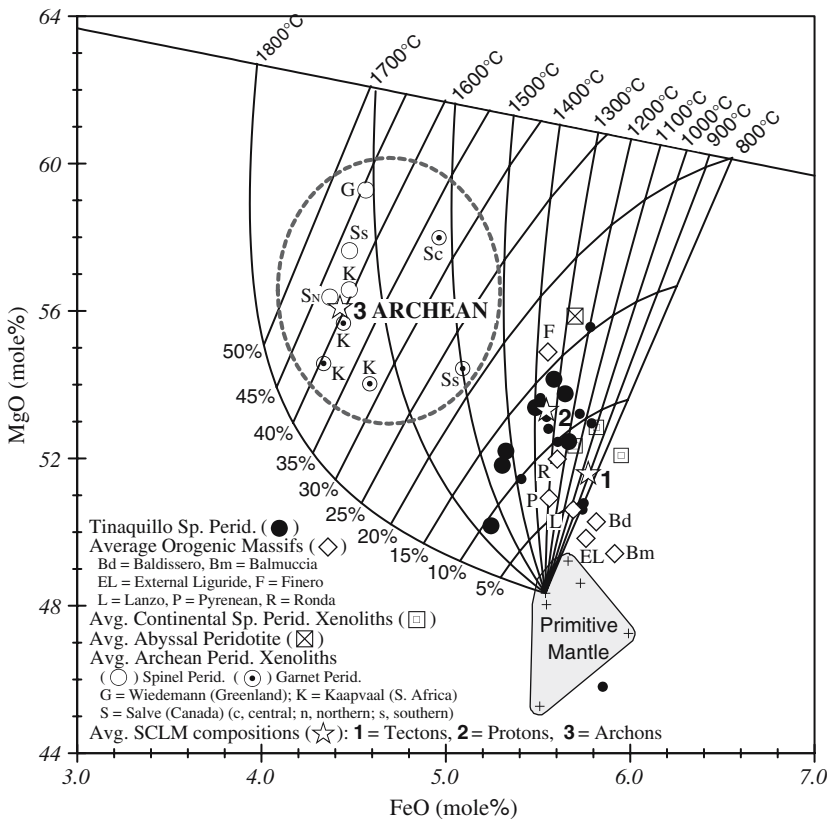

Fig. 6 Calculated FeO and MgO concentrations in residues generated by partial melting of a primitive mantle source. The diagram is contoured for temperature and degree of batch melting of primitive mantle at 2.5 GPa, after Hanson and Langmuir (1978). The distribution coefficient of $(Fe/Mg)_{ol}/(Fe/Mg)_{melt}$ determined by Grover et al. (1980) is used. All Fe was assumed to be Fe^{2+}. Data sources for the primitive mantle, average continental spinel peridotites, average abyssal peridotite, Alpine orogenic massifs, and Tinaquillo peridotites (*small circle*) as in Fig. 2. Average Archean peridotite xenolith compositions are from Boyd (1989), Bernstein et al. (1998), Griffin et al. (1999), Kopylova and Russell (2000), and Kopylova and Caro (2004), and the average SCLMs are from Griffin et al. (1999)

alpine-type peridotites thought to have originated as parts of the SCLM, such as the Balmuccia, Baldissero, and Lanzo massifs in the Italian Alps (Bodinier 1988; Hartmann and Wedepohl 1993; Mukasa and Shervais 1999), External Liguride massif in the Northern Apennines, Italy (Rampone et al. 1995), Eastern Pyrenean massifs of southern France (Bodinier et al. 1988), and Ronda massif in SE Spain (Frey et al. 1985). However, Tinaquillo peridotites are less depleted compared to the average abyssal peridotite, and Finero massif in the Italian Alps, which is a known example of sub-arc peridotite fluxed with subduction components (Hartmann and Wedepohl 1993; Griffin et al. 1999) (Fig. 2).

In Fig. 6, we have shown the calculated FeO and MgO concentrations in partial melting residues generated by melting of a primitive mantle source at P = 2.5 GPa, following Hanson and Langmuir (1978), and have compared these with the compositions of other well-studied peridotites. Tinaquillo peridotites have MgO and FeO contents consistent with calculated residues formed by 9–15% melting of a primitive mantle, which in general is higher than the degree of melting inferred for orogenic peridotites originating in the SCLM, but lower than estimates for arc settings (e.g., Finero massif) and abyssal peridotites.

Ruling out an arc-origin for the Tinaquillo peridotites, as first proposed by Seyler and Mattson (1989) is confirmed by the cr# [=100Cr/(Cr + Al)] of spinel grains from the Tinaquillo peridotites which have a range of 9.8–24.2. Such values indicate significantly lower degrees of partial melting compared to arc peridotites typified by cr#s of ~38 to over 80 (Dick and Bullen 1984; Gaetani and Grove 1998). The cr#s of Tinaquillo spinel grains are also lower than those of abyssal peridotites which generally range from 13 to 57 (Dick and Bullen 1984). Furthermore, Tinaquillo peridotite moderately incompatible elements, like $(Yb)_N$, (1.71 ± 1.08; n = 7, 1σ) (Table 1), is higher than what is observed in the Finero SSZ peridotites (0.34 ± 0.20; n = 11, 1σ) (Hartmann and Wedepohl 1993), sub-oceanic lithospheric mantle (SOLM) peridotites from Internal Liguride (Northern Apennines, Italy) (1.31 ± 0.83; n = 3, 1σ) (Rampone et al. 1996) (Fig. 3a), and mantle wedge peridotite xenoliths from Papua New Guinea (0.15 ± 0.07; n = 4, 1σ) (Grégoire et al. 2001).

For peridotite xenoliths from lithosphere stabilized in the Archean, materials derived from the spinel stability field in the shallow mantle show greater chemical depletion than is observed in garnet peridotite from the deeper mantle (Fig. 6). Tinaquillo spinel peridotites match well with the mean composition for Proton SCLM in Fig. 6. Most of the SCLM-derived orogenic peridotite massifs compared in this study were stabilized as part of Phanerozoic lithospheric sections (e.g., Griffin et al. 1999; Downes 2001 and references therein). However, Reisberg et al. (1991) suggested an age of 1.2 Ga for the time at which the Ronda massif in southern Spain left the convecting asthenosphere and became incorporated into the lithosphere, and Burnham et al. (1998) obtained an Os model age for mantle depletion of ~1.9 Ga in a study of eastern Pyrenean ultramafic massifs. These observations suggest that the Tinaquillo peridotite is a fragment of the SCLM, possibly isolated from the convecting asthenosphere in the early Proterozoic as argued with isotopic data immediately below.

In Fig. 5a, we have compared the available Sr and Nd isotopic compositions of present-day values for clinopyroxene separated from several alpine-type orogenic peridotites to those of some Tinaquillo peridotites. The Tinaquillo peridotites have Nd isotopic compositions that overlap with those of present-day MORB, but extending to values more radiogenic (i.e., depleted) than MORB. This contrasts markedly with the Nd ratios of other alpine-type orogenic peridotites, which overlap with MORB but then extend to values more enriched than Bulk Earth. It can therefore be argued that the commonly invoked processes of time-integrated enrichments in LREE, due to reaction with infiltrated melts/fluids derived from enriched mantle sources and/or continental crust during emplacement into crust were not operative in the geochemical evolution of the Tinaquillo massif. Sample TQ-11 in particular has extremely depleted Nd (ε_{Nd} = +27) and Hf (ε_{Hf} = +50) isotopic compositions (Tables 2, 3), far more so than even the Internal Liguride peridotite thought to represent Permian sub-oceanic lithospheric mantle (SOLM) for which ε_{Nd} values range between +19 and +22 (Rampone et al. 1996). These extreme isotopic compositions are confirmed by the Nd and Hf isotopic determinations on an ultra-pure clinopyroxene separate from sample TQ-11 for which ε_{Nd} and ε_{Hf} are +26 and +48, respectively (Tables 2, 3) and plot along the Nd–Hf mantle array in Fig. 5b. Such highly radiogenic Hf isotopic compositions have also been reported for spinel peridotite xenolith clinopyroxenes from Salt Lake crater, Hawaii (ε_{Hf} = +58 – +66; Bizimis et al. 2003). However, the Hawaiian peridotite clinopyroxenes display extreme decoupling in the Hf and Nd isotopic values such that $\Delta\varepsilon_{Hf}$ = +45 – 51, which has been interpreted as the result of metasomatism by the host alkali basaltic melts (Salters and Zindler 1995; Bizimis et al. 2003). The coupled, extremely radiogenic Nd and Hf isotopic compositions of sample TQ-11 are likely to be due to long-term radiogenic ingrowth after

melt extraction in the sub-continental lithospheric mantle. The Nd model age (T_{DM}) of this sample is ca. 3.4 Ga (Table 2), based on the assumptions that (1) the mantle domain from which the sample originated experienced only single-stage depletion, and (2) the depleted mantle (DM) evolves in a simple linear fashion that is not impacted appreciably by younger melting events. Interestingly, sample TQ-11 has the highest concentrations of basaltic components, such as Al_2O_3 and CaO, among the samples studied (Table 1), which might indeed exclude the possibility of multiple episodes of melt extraction, and instead favor simple, single-stage melting.

However, the Nd model age of ca. 3.4 Ga is somewhat imprecise because of the small range in $^{147}Sm/^{144}Nd$ ratios and closeness of the data points to the Chondritic Uniform Reservoir (CHUR) composition. In addition, although the evolution of DM through time is still not fully constrained, there is a strong possibility that the DM Nd isotopic evolutionary trend—derived from the mid-ocean ridge basalts today, and Proterozoic–Phanerozoic juvenile mantle-derived rocks—might not extend into the Archean in a linear fashion. It has been argued that a transition may have developed around 3.7 Ga that decouples Archean from Proterozoic evolution of the depleted mantle (Bennett et al. 1993; Vervoort et al. 1996; Vervoort and Blichert-Toft 1999). If this model is correct, then Nd model ages extending into the Archean turn out to be older than they should be. The extremely depleted Nd and Hf isotopic compositions may be indicative of an earlier depletion event in this massif at mantle pressures, possibly during the Early Proterozoic.

Subduction-related metasomatism for the Tinaquillo peridotites

The Tinaquillo peridotites show a LREE depletion characterized by $(Ce)_N < 1$ (Fig. 3a), similar to anhydrous alpine-type peridotites as shown in Fig. 3a. However, TQ-4, the most HREE-depleted sample among all those studied, has the highest LREE concentrations (Table 1) in spite of having the lowest Yb, leading to an inverse correlation between $(Ce)_N$ and $(Yb)_N$ (Fig. 3a), and between Sr and Yb (Fig. 3b). These characteristics are not consistent with simple melt extraction, but instead reflect some overprinting by secondary cryptic metasomatic event(s) in the history of the massif. This is a widespread phenomenon observed in anhydrous peridotite xenoliths in continental settings (e.g., Ionov et al. 2002; Choi et al. 2005). The most depleted portions of the peridotite are more susceptible to modification by the metasomatic agent than the less depleted parts, due to their lower concentration level and/or higher permeability (Toramaru and Fujii 1986; Bedini et al. 1997). However, the relative enrichment in LREEs or Sr in the Tinaquillo peridotites is much weaker than it is in the Finero SSZ peridotites. Finero experienced repeated episodes of melt extraction and strong re-enrichment(s) by silicic melts from a subduction zone, resulting in pervasive hydrous modal metasomatism with development of phlogopite and amphibole (e.g., Hartmann and Wedepohl 1993) (Fig. 3a, b).

The element distribution diagram for the Tinaquillo peridotites in Fig. 4a shows a well-developed Th trough relative to Ba and U, as well Pb enrichment over adjacent REEs, similar to arc basalts, as shown in Fig. 4b. The characteristic enrichment in the hydrophile element U over Th is attributed to the preferential mobility of U in slab-derived fluids (e.g., Bizimis et al. 2000). These characteristics match well with the unusually radiogenic Sr for some samples, falling to the right of the Sr–Nd mantle array (Fig. 5a), owing to subduction fluids containing relatively high concentration of Sr, but very little Nd. Therefore, the effect of these fluids on the mantle peridotite—especially for the low Sr concentrations exhibited by the Tinaquillo peridotite—is extreme elevation in $^{87}Sr/^{86}Sr$, even in cases of only mild overprinting.

Subduction-zone fluids are derived from seawater-altered basalts and sea-floor sediments. Lead isotopes are more sensitive than Sr, Nd and Hf isotopes to the addition of a small sedimentary component, because Pb concentrations in sediments (~20 ppm; McCulloch and Gamble 1991) and altered MORB (~0.3 ppm; McCulloch and Gamble 1991) are distinct compared to the Nd, Hf, and even Sr concentrations in the two materials (e.g., for Sr, ~1,000 ppm vs. ~110 ppm; McCulloch and Gamble 1991, and references therein). Note that the concentrations of Pb and Sr in sediments and altered MORB are different by factors of ~70 and ~10, respectively. Therefore, subduction-related fluids may have distinctive Pb isotope signatures if the sea-floor sediments have been derived from old crustal rocks. For the Tinaquillo peridotites, metasomatic fluid derived from seawater-altered basalts is plausible. The associated sea-floor sediments are not likely to be a major component in the source considering that their $^{207}Pb/^{204}Pb$ and $^{208}Pb/^{204}Pb$ ratios at a given value of $^{206}Pb/^{204}Pb$ are not reflected in the compositions of the metasomatized peridotites.

Figure 5a shows a simple binary mixing curve for Sr and Nd isotopes between hydrothermally altered-MORB (A-MORB on the diagram) and a residual peridotite (RP) protolith. In the calculation, we have

assumed the residual peridotite to have: Sr = 1 ppm, Nd = 0.25 ppm, $^{87}Sr/^{86}Sr$ = 0.70125, and $^{143}Nd/^{144}Nd$ = 0.51410. We have also included two end-member situations of slab-derived fluids with: (1) Sr = 2,933 ppm, Nd = 146 ppm as first proposed by Tatsumi and Kogiso (1997) (ML_{TK} in Fig. 5a), and (2) Sr = 150 ppm, Nd = 1,930 ppm from the work of Bizimis et al. (2000) ($ML_{B\text{-}min}$ in Fig. 5a). Sr and Nd isotopic compositions of altered MORB-derived fluid ($^{87}Sr/^{86}Sr$ = 0.70125, and $^{143}Nd/^{144}Nd$ = 0.51410) are taken from Tatsumi and Kogiso (1997). The simple mixing calculation indicates that an addition of <3% of hydrous fluid can account for the Sr–Nd systematics of the Tinaquillo peridotites, without affecting the major element geochemistry.

The Sm–Nd isotope data for the Tinaquillo peridotites do not produce highly collinear arrays (Fig. 7a), which means that the mixing between residual peridotite protolith and hydrous fluid did not involve a mere two end-members, each intrinsically homogeneous. The effects of relatively recent fluid enrichment can be discerned in the low $^{147}Sm/^{144}Nd$ but high $^{143}Nd/^{144}Nd$ ratios compared with the DM-like samples TQ-4 and TQ-13. Recent fluid enrichment is likely to have caused the decrease in $^{147}Sm/^{144}Nd$ (LREE enrichment) while also altering the $^{143}Nd/^{144}Nd$ ratio towards that of the metasomatizing agents. Considering that sample TQ-4 with a $^{143}Nd/^{144}Nd$ ratio of 0.513095 ± 24 (ε_{Nd} = +9) has the lowest $^{147}Sm/^{144}Nd$ ratio among the samples studied, we can then surmise that the metasomatic agents originated from the subducted altered oceanic lithosphere, which is consistent with the idea of a slab-derived fluid. Among the peridotite samples analyzed, only TQ-4, TQ-10, and TQ-16 define an errorchron of 153 Ma while four other samples fall above this line in a scattered pattern (Fig. 7a). The errorchron is in remarkably good agreement with the reported zircon U–Pb concordia upper intercept age of 150 ± 2 Ma (Seyler et al. 1998) for a felsic dike that cuts the Tinaquillo massif. Also of note, the Nd isotopic compositions of the Tinaquillo peridotites are not well correlated with their levels of fertility in basaltic components (Tables 1, 2). Therefore, the partial resetting of the Sm–Nd clock recorded in the peridotites suggests that hydrous fluid transport in the massif is most likely to have been by channelized flow rather than wholesale percolation.

We have noted that the whole-rock Sr isotopic composition for sample TQ-11 does not match that of the clinopyroxene, notwithstanding the agreement in their Pb isotopic compositions (Table 2). However, the significantly unradiogenic Sr isotopic composition of the clinopyroxene—at least relative to the whole-rock—still falls off the Sr–Nd mantle array (Fig. 5a). The Pb diffusion coefficient in diopside is ~10^{-22} m^2/s at 900°C (Cherniak 2001), which is comparable to the values for Sr diffusion (~10^{-20}–10^{-24} m^2/s, Sneeringer et al. 1984). Therefore, it is reasonable to suggest that the observed lack of Sr isotopic equilibrium has survived because of the slowness of diffusion following the secondary overprinting by subduction-zone fluids enriched in Sr and Pb, but also that this event must have occurred only recently in the long history of these mantle materials, possibly during the Late Jurassic. Re-equilibration in the Pb isotopes between clinopyroxene and the rest of the peridotite—but not the Sr

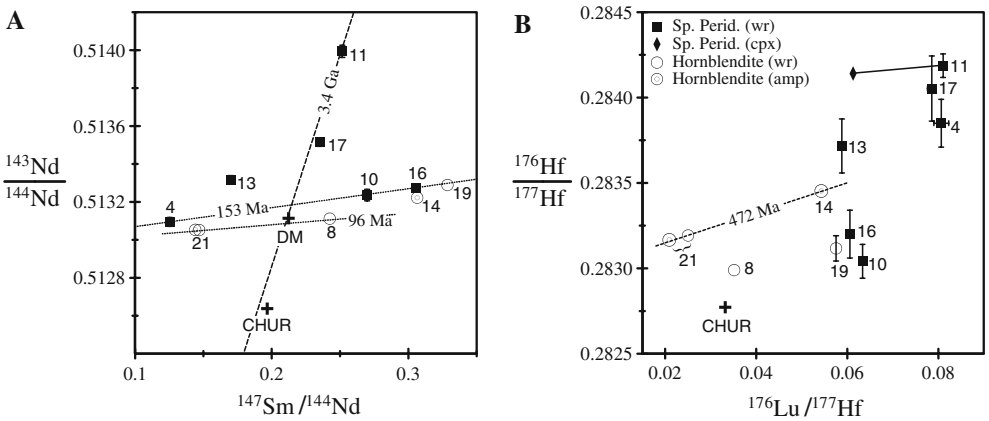

Fig. 7 **a** $^{143}Nd/^{144}Nd$ versus $^{147}Sm/^{144}Nd$, and **b** $^{176}Hf/^{177}Hf$ versus $^{176}Lu/^{177}Hf$ systematics of the Tinaquillo peridotites and hornblendite veins. All error bars are 2σ uncertainties, and are given only where they exceed the size of the symbol in the plot. The *dashed lines* are reference isochrons. The decay constant $\lambda^{176}Lu = 1.865 \times 10^{-11}$ $year^{-1}$ (Scherer et al. 2001) has been used to calculate the Lu–Hf errorchron in B. The present-day CHUR parameters are from Blichert-Toft and Albarède (1997). *wr* whole-rock; *cpx* clinopyroxene; *amp* amphibole

isotopes—is likely to be an interplay between diffusion coefficients and the relative abundances of Sr and Pb within the channelized fluid supply.

Hafnium mobility in slab-derived fluid

Arc magmatism is characterized by strong depletion in Nb and Ta relative to the large-ion lithophile elements (LILE) such as K, Rb, Ba, U and Th (e.g., McCulloch and Gamble 1991), and overall, low concentrations in all the high-field-strength elements (HFSE)—Nb, Ta, Zr, Hf and Ti. The HFSE are thus generally believed to be immobile during slab dehydration reactions, although subtle partitioning seems required for the negative anomalies in Zr, Hf and Ti which are usually less extreme than those observed for Nb and Ta.

For an understanding of the timing of Tinaquillo peridotite separation from the convecting mantle, we have conducted Lu–Hf systematics with the assumption that this parent–daughter system might remain robust during the secondary metasomatic event(s) compared to the fluid-mobile LREE (e.g., Nd) (Pearson and Nowell 2003, 2004). However, the Lu–Hf isotope data for the Tinaquillo peridotites, contrary to expectation, do not show a clear isochron (Fig. 7b), even taking into account the large uncertainty in the Hf isotopic ratios for some of the samples. Peridotite samples TQ-10 and TQ-16 with clear resetting in the Sm–Nd system that we have attributed to slab-derived fluids (Fig. 7a), plot within the range for MORB on the $^{176}Hf/^{177}Hf$ versus $^{143}Nd/^{144}Nd$ correlation diagram (Fig. 5b), which indicates modification of the Hf isotopic compositions in these two samples by hydrous fluids. In a study of Lu–Hf systematics of oceanic arc lavas, Woodhead et al. (2001) suggested that Hf is mobile in subduction zones and may even be fluid mobile, supporting our observation.

In Fig. 5b, we have shown a simple binary mixing curve between hydrothermally altered-MORB and residual peridotite protolith for Nd and Hf isotopes. The Nd concentration and isotopic compositions used for the two end-members are the same as in Fig. 5a. The Hf concentration for altered-MORB is taken to be a factor of 2 higher than that in N-MORB (2.05 ppm; Sun and McDonough 1989) based on work by Jochum and Verma (1996), and that for residual peridotite is assumed to be 0.05 ppm. The $^{176}Hf/^{177}Hf$ ratios for the two end-members have been chosen arbitrarily with the interest of considering the likely extreme compositions (0.28420 for residual peridotite; 0.28300 for altered MORB). Due to a lack of data on Hf concentrations in hydrous fluids, we have calculated one using two approaches we consider to be quite reasonable. In the first, we have used the $D^{slab/fluid}$ values for Hf, which have been calculated from the modal abundances of the slab, namely 59% garnet, 40% clinopyroxene and 1% rutile (Ayers 1998), and the experimentally determined Hf partition coefficients on garnet/hydrous fluid and clinopyroxene/hydrous melt (Green et al. 2000), and rutile/hydrous fluid (Brenan et al. 1994) (mixing line 1, ML_1, in Fig. 5b). In the second, we have adopted the calculation by Tatsumi and Kogiso (1997) for which the mobility of Hf in hydrous fluid is based on the value for Ti (Kogiso et al. 1997), assuming similar behavior by Hf and Ti in the fluid (ML_2 in Fig. 5b). The simple mixing calculation indicates that an addition of <~2% of hydrous fluid can account for the Nd–Hf systematics of the Tinaquillo peridotites, even with the extreme compositions we have considered.

However, it should be stressed that all of the Tinaquillo peridotites have $^{176}Lu/^{177}Hf$ ratios higher than CHUR, and that samples TQ-4, TQ-10, and TQ-16 which define a Sm–Nd errorchron of 153 Ma do not produce one in the Lu–Hf system (Fig. 7a, b). These results suggest that the mobility of Hf in the hydrous fluid is feeble compared to the mobility of LREEs. The peridotite Hf isotopic compositions do not show a discernable correlation with fertility in the basaltic components, such as CaO and Al_2O_3 (Tables 1, 3). Furthermore, the Hf concentrations in the Tinaquillo peridotites of ≤0.12 ppm are extremely low when compared with the average spinel peridotite xenolith composition of ~0.27 ppm (e.g., McDonough 1990). The low concentration level of Hf in the Tinaquillo peridotites has rendered these rocks to be susceptible to overprinting by the hydrous fluids that induced metasomatism.

Partial melting in the garnet stability field for the Tinaquillo peridotites

The Tinaquillo bulk peridotite compositions display negative Ti anomalies relative to the adjacent elements (Fig. 4a). While the depletion in Ti relative to REE could be considered a signature of carbonatitic metasomatism (Yaxley et al. 1998), we rule out that possibility in this case because (1) the fractionated HREE pattern (Fig. 4a) is inconsistent with that model, especially for the least metasomatized sample TQ-11 which has the highest HREE and lowest LREE concentrations, as well as most radiogenic Hf and Nd among the samples studied (Fig. 4a); (2) there are no Hf and Nb negative anomalies (Fig. 4a); and (3) CaO/Al_2O_3 ratios of the Tinaquillo peridotites (0.84–0.96 with average 0.91; Table 1) are similar to the 0.95 value for average

subcontinental lithosphere of McDonough (1990). This is not as high, for example, as the average value of 2.62 for SE Australian peridotites metasomatized by carbonatites (Yaxley et al. 1998). Experimentally determined Ti partition coefficients on garnet/basaltic melt are relatively low compared to those of the neighboring elements—Eu and Tb (e.g., Hauri et al. 1994; Green et al. 2000), which means that garnet was a possible residual phase after partial melting. The fact that no garnet is observed in the Tinaquillo peridotites implies that this mineral was subsequently destroyed in decompression-driven, subsolidus reactions at spinel-facies conditions prior to the incorporation of the massif into the crust. This interpretation matches well with the highly fractionated HREE. In Fig. 3a and b, we have shown the calculated Ce versus Yb, and Sr versus Yb compositional trends for the residues of a fractional/equilibrium melt extraction from primitive mantle compositions (Sun and McDonough 1989) within the garnet stability field. The marked depletion in Ce and Sr concentration levels of sample TQ-11 at a given Yb content can be explained in terms of the rock being a residue of low degrees of fractional melt extraction in the garnet stability field, similar to the Internal Liguride peridotite (Fig. 3a, b), for which this process has been invoked (Rampone et al. 1996). In addition, the low Sr concentrations in most Tinaquillo peridotites are explained well by the fractional melting residue model and subsequent cryptic metasomatism by hydrous fluids.

Tectonic framework for the Tinaquillo complex during the Late Jurassic to Mid-Cretaceous

The Nd and Hf isotopic compositions of the Tinaquillo hornblendite veins fall within the range for Pacific/Atlantic MORB on the $^{143}Nd/^{144}Nd$ versus $^{176}Hf/^{177}Hf$ correlation diagram (Fig. 5b), whereas compositions for the host peridotites range from the MORB field to values even more depleted than MORB. Furthermore, the host peridotites record unusually radiogenic Sr, falling to the right of the mantle array on the Sr–Nd correlation diagram (Fig. 5a), a characteristic that the hornblendites do not possess. These observations suggest that (1) the Tinaquillo peridotites are not the mantle source for the magmatism that produced the hornblendite veins, and (2) addition of highly radiogenic Sr to selected domains within the peridotites by slab-derived fluids occurred prior to the vein emplacement. That is to say, the Tinaquillo peridotites appear to have remained at temperature below the dry solidus during the hornblendite magmatism. On the $^{147}Sm/^{144}Nd$ versus $^{143}Nd/^{144}Nd$ (Fig. 7a), and $^{176}Lu/^{177}Hf$ versus $^{176}Hf/^{177}Hf$ (Fig. 7b) isochron diagrams, the hornblendites do not consistently define any meaningful isochrons. For example, samples TQ-8 and TQ-21 define an errorchron of ~96 Ma on the Sm–Nd isochron diagram, but produce an unrealistic future age in the Lu–Hf system. It should be pointed out that the Sm–Nd isotope data for the hornblendites do not fall on the 153 Ma errorchron defined by the three peridotites described earlier (Fig. 7a), perhaps not proving but consistent with the idea that the slab-derived fluid was added to the peridotites prior to hornblendite emplacement, possibly in Late Jurassic. We propose that the hornblendite veining occurred during the Mid-Cretaceous as shall be argued below.

On the element distribution diagram shown in Fig. 4b, our new data have been plotted in comparison with the compositions for N-MORB, typical arc basalt, and previously determined elemental concentrations for a Tinaquillo gabbroic granulite. The hornblendites show the ''arc-signature,'' such as the Sr spike, as well as Nb and Th troughs compared to adjacent elements, and the HREE depletion relative to N-MORB. However, depletion of LILEs in the hornblendites is contrary to an arc origin, and instead is explicable by derivation from the depleted MORB source. The Tinaquillo gabbroic granulite has also shown the characteristic geochemistry, a mixture of arc-like and MORB-like end members (Fig. 4b). In addition, the presence of hornblende in the granulites (Seyler and Mattson 1993; Seyler et al. 1998) is indicative of a relatively high volatile content in the mantle source.

Based on these observations, we have formulated a tectonic framework for the Tinaquillo Complex during the Late Jurassic to Mid-Cretaceous, as shown in Fig. 8. It has already been demonstrated that opening of the Protocaribbean Sea by spreading between North and South American Plates began in Early Jurassic (e.g., Kerr et al. 1999). The northwestern margin of the South America Plate (SAP) where the Tinaquillo Complex was to be emplaced has been bounded by the Andes of western Venezuela along the NE–SW-trending right-lateral strike-slip Boconó fault (BF in Fig. 1a) since the Miocene (Pindell et al. 1988; Audemard and Audemard 2002). Most plate tectonic models for the evolution of the Caribbean Plate (CP) assume a Pacific (Farallon) origin, and transport into its present location by significant eastward plate movements (e.g., Pindell 1993; Sinton et al. 1998; Smith et al. 1999). We propose that the Tinaquillo Complex originated from the northwestern margin of the SAP, which is in accord with the larger-scale models for Caribbean Plate–South American Plate interactions. We further propose that the Tinaquillo peridotites

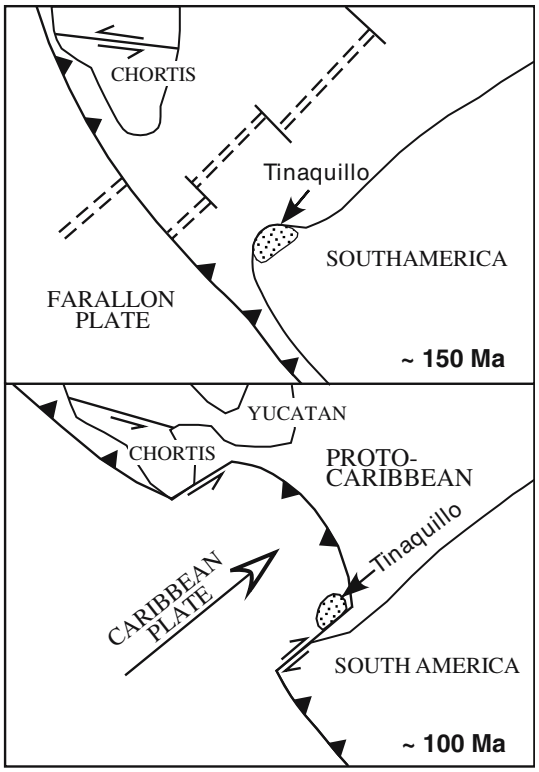

Fig. 8 Two map views at 150 Ma (Late Jurassic) and 100 Ma (Mid-Cretaceous) illustrating the tectonic model most consistent with the geochemical evidence presented here for the metasomatic and mafic melt incorporation into the Tinaquillo Complex, based in part on the ideas of Pindell et al. (1988) and Smith et al. (1999)

represent refractory SCLM, genetically coupled with the Guiana Shield (Fig. 1d), one of the two world's most extensive domains of Proterozoic crust—the Trans-Amazonian granitoids-greenstone belts, yielding ages between 2.25 and 2.08 Ga (e.g., Teixeira et al. 1989; Norcross et al. 2000; Voicu et al. 2001).

Based on the major element geochemistry, and the Nd and Hf isotopic compositions, especially of sample TQ-11 (ε_{Nd} = +27; ε_{Hf} = +50; Nd model age ≈ 3.4 Ga) (see details above) we rule out the alternative possibilities of origination of the Tinaquillo complex in the Andean supra-subduction zone or as a sub-oceanic lithospheric mantle with affinities to the interactions between the Protocaribbean and Farallon plates. In our proposed model, during Late Jurassic time, the tectonic setting of the Farallon Plate subducting beneath the SAP had modified the refractory Tinaquillo peridotites, which at the time were superjacent to the slab, by the subduction-related channelized hydrous flux.

Most models of Caribbean plate motion invoke a subduction polarity reversal, for which timing is not yet well-constrained, but with estimates ranging from 120 to 60 Ma (Burke 1988; Draper et al. 1996; Pindell et al. 2005). Pindell (1993) suggested that this reversal to westward-dipping subduction occurred in response to a sudden increase in spreading rates in the Atlantic at around 100 Ma. Others (e.g., Burke et al. 1984; Duncan and Hargraves 1984; White et al. 1999) argued that the arrival of the 88–91 Ma plume-related Caribbean plateau and its collision with the Proto-Grater Antilles Arc clogged the subduction zone and caused the polarity reversal. This polarity change caused a segment of the Farallon Plate to evolve into a 'promontory' that became the transform-bounded Caribbean Plate, which along with the Great Arc of the Caribbean then migrated northeastward with respect to North America and South America, and the Protocaribbean lithosphere then began to be subducted beneath the Caribbean Plate (Burke 1988; Pindell 1993; Smith et al. 1999).

We suggest that during inception of the westward-dipping subduction of the relatively young Protocaribbean oceanic plate, immediately following polarity reversal in the Mid-Cretaceous, melts infiltrated the mantle lithosphere and produced the Tinaquillo hornblendite veins and the Tinaquillo gabbroic intrusions. Stern and Bloomer (1992) argued that the earliest stage of subduction initiated strong fore-arc extension, in many ways indistinguishable from that of sea-floor spreading. Therefore, the combined effects of the adiabatic decompression of the asthenosphere triggered by this extension plus the lowering of the peridotite solidus by the influx of water induced the melting that produced arc-like magmas.

The geodynamic setting of the Tinaquillo Peridotite Massif during the Late Jurassic to Mid-Cretaceous was explained by Seyler et al. (1998) as involving (1) a subcontinental lithospheric block getting left between the North American and South American Plates during the N–S-spreading that formed the Protocaribbean oceanic basin, (2) block modification during back-arc development, while positioned between an eastward subducting Farallon Plate and the N–S-spreading Protocaribbean oceanic rift, and (3) emplacement of the Tinaquillo hornblendite veins as by-products of subduction of the Protocaribbean Ridge.

We offer a new model that is more in accord with the larger-scale models for Caribbean Plate–South American Plate interactions, and in light of the data presented here, wherein: (1) the Tinaquillo Peridotite Massif originates from the northwestern margin of the SAP, as part of the Guiana Shield; (2) transform-bounded transposition of the Caribbean Plate eastwards facilitated by a subduction polarity reversal decouples the massif from the SAP; (3) hornblendite

veining results from emplacement of magmas produced during the earliest stages of westward subduction of the Protocaribbean Plate; and (4) exhumation occurred in a transpressional stress regime involving SAP–Caribbean Plate interactions during the Late Eocene to Mid-Miocene.

Coexistence of arc- and depleted MORB-related trace element signatures in the Tinaquillo hornblendites is consistent with this model, as are the isotopic differences, especially in $^{87}Sr/^{86}Sr$ ratios, between the peridotites and hornblendites. The Sr and Nd isotopic compositions of the hornblendites, which fall in the range for present Pacific/Atlantic MORB, are significantly different compared to the 88–91 Ma plume-related Caribbean oceanic plateau, here represented by Curaçao and Aruba lavas (Fig. 1a), obducted in the southern Caribbean. These lavas have ε_{Nd} = +5.7 to +7.8 (Sinton et al. 1998; White et al. 1999), indicating that the hornblendite magmatic activity had ceased by the time that the plume-related plateau magmatism commenced. Based on the 96-Ma peak metamorphism observed in the Villa de Cura blueschist belt (Fig. 1b), Smith et al. (1999) argued that the belt formed in Mid-Cretaceous time in an intra-oceanic subduction zone setting in which Protocaribbean lithosphere was subducted beneath the Caribbean Plate. These observations support an older (~100 Ma) age for reversal of the subduction zone polarity for the Caribbean (Pindell 1993). The relative northward movement of the Caribbean Plate continued until the Eocene, when the CP collided with the Bahama platform. Since then, the plate has moved east or southeastward relative to the North American and South American plates facilitating emplacement of the Tinaquillo Complex onto the South American continent.

Conclusions

1. The Tinaquillo spinel peridotite massif is a fragment of the sub-continental lithospheric mantle with affinities to the Guiana Shield (South America), isolated from the convecting asthenospheric mantle possibly in the Early Proterozoic.
2. Fractional melting initiated within the garnet stability field is the best model to explain the trace element concentrations of the Tinaquillo peridotites.
3. Hornblendite veins that cut the Tinaquillo peridotite have less radiogenic Hf, Nd and Sr isotopic compositions, making it unlikely that they were produced by local melting of the host peridotite rocks.
4. The Tinaquillo peridotites have elevated Sr isotopic compositions, falling off on the Sr–Nd mantle array, a feature not shared by the hornblendite veins. The peridotite therefore must have acquired this signature prior to vein emplacement.
5. We attribute the origin of the hornblendite veins to mantle melting during inception of the westward-dipping subduction of the Protocaribbean Plate, immediately following polarity reversal in the Mid-Cretaceous. Infiltration of Farallon Plate subduction-derived channelized fluids into the Tinaquillo peridotites, in the Late Jurassic, is considered to be the most likely source of the arc signature that imprinted the residual protoliths.
6. The Tinaquillo complex was emplaced into the southern Caribbean belt as a result of convergence between the North and South American Plates during the Late Eocene to Mid-Miocene.

Acknowledgements This work was supported by the National Science Foundation grant (EAR-049532) to SBM. We would like to thank T.L. Grove, and two anonymous reviewers for their constructive reviews

References

Audemard FE, Audemard FA (2002) Structure of the Mérida Andes, Venezuela: relations with the South America–Caribbean geodynamic interaction. Tectonophysics 345: 299–327

Andres M, Blichert-Toft J, Schilling J (2004) Nature of the depleted upper mantle beneath the Atlantic: evidence from Hf isotopes in normal mid-ocean ridge basalts from 79°N to 55°S. Earth Planet Sci Lett 225:89–103

Ayers J (1998) Trace element modeling of aqueous fluid-peridotite interaction in the mantle wedge of subduction zones. Contrib Mineral Petrol 132:390–404

Beard BL, Johnson CM (1993) Hf isotope composition of late Cenozoic basaltic rocks from northwestern Colorado, USA: new constraints on mantle enrichment processes. Earth Planet Sci Lett 119:495–509

Bedini RM, Bodinier J-L, Dautria J-M, Morten L (1997) Evolution of LILE-enriched small melt fractions in the lithospheric mantle: a case study from the East African Rift. Earth Planet Sci Lett 153:67–83

Bennett VC, Nutman AP, McCulloch MT (1993) Nd isotopic evidence for transient, highly depleted mantle reservoirs in the early history of the Earth. Earth Planet Sci Lett 119:299–317

Bernstein S, Kelemen PB, Brooks CK (1998) Depleted spinel harzburgite xenoliths in Tertiary dykes from East Greenland: restites from high degree melting. Earth Planet Sci Lett 154:221–235

Bizimis M, Salters VJM, Bonatti E (2000) Trace and REE content of clinopyroxenes from supra-subduction zone peridotites: Implications for melting and enrichment processes in island arcs. Chem Geol 165:67–85

Bizimis M, Sen G, Salters VJM (2003) Hf–Nd isotope decoupling in the oceanic lithosphere: constraints from spinel peridotites from Oahu, Hawaii. Earth Planet Sci Lett 217:43–58

Blichert-Toft J, Albarède F (1997) The Lu–Hf isotope geochemistry of chondrites and the evolution of the mantle-crust system. Earth Planet Sci Lett 148:243–258

Blichert-Toft J, Frey FA, Albarède F (1999) Hf isotope evidence for pelagic sediments in the source of Hawaiian basalts. Science 285:879–882

Blichert-Toft J, Agranier A, Andres M, Kingsley R, Schilling J, Albarède F (2005) Geochemical segmentation of the Mid-Atlantic Ridge north of Iceland and ridge-hot spot interaction in the North Atlantic. Geochem Geophys Geosys 6:1–27

Bodinier J-L (1988) Geochemistry and petrogenesis of the Lanzo peridotite body, western Alps. Tectonophysics 149:67–88

Bodinier J-L, Dupuy C, Dostal J (1988) Geochemistry of petrogenesis of Eastern Pyrenean peridotites. Geochim Cosmochim Acta 52:2893–2907

Bodinier J-L, Menzies MA, Thirlwall MF (1991) Continental to oceanic mantle transition–REE and Sr–Nd isotopic geochemistry of the Lanzo lherzolite massif. J Petrol Spec Lherz Issue, pp 191–210

Bodinier J-L, Vasseur G, Vernieres J, Dupuy C, Fabries J (1990) Mechanism of mantle metasomatism: geochemical evidence from the Lherz orogenic peridotite. J Petrol 31:597–628

Boyd FR (1989) Compositional distinction between oceanic and cratonic lithosphere. Earth Planet Sci Lett 96:15–26

Brenan JM, Shaw HF, Phinney DL, Ryerson FJ (1994) Rutile–aqueous fluid partitioning of Nb, Ta, Hf, Zr, U and Th: implications for high field strength element depletions in island-arc basalts. Earth Planet Sci Lett 128:327–339

Burke K (1988) Tectonic evolution of the Caribbean. Ann Rev Earth Planet Sci 16:201–230

Burke K, Cooper C, Dewey JF, Mann P, Pindell JL (1984) Caribbean tectonics and relative plate motions. In: Bonini WE, Hargraves RB, Shagam R (eds) The Caribbean–South American Plate Boundary and regional tectonics. Geol Soc Am Mem 162:31–63

Burnham OM, Rogers NW, Pearson DG, van Calsteren PW, Hawkesworth CJ (1998) The petrogenesis of the eastern Pyrenean peridotites: an integrated study of their whole-rock geochemistry and Re–Os isotope composition. Geochim Cosmochim Acta 62:2293–2310

Chauvel C, Blichert-Toft J (2001) A hafnium isotope and trace element perspective on melting of the depleted mantle. Earth Planet Sci Lett 190:137–151

Cherniak DJ (2001) Pb diffusion in Cr diopside, augite, and enstatite, and consideration of the dependence of cation diffusion in pyroxene on oxygen fugacity. Chem Geol 177:381–397

Choi SH, Kwon S-T, Mukasa SB, Sagong H (2005) Sr–Nd–Pb isotope and trace element systematics of mantle xenoliths from Late Cenozoic alkaline lavas, South Korea. Chem Geol 221:40–64

Choi SH, Mukasa SB, Kwon S-T, Andronikov AV (2006) Sr, Nd, Pb and Hf isotopic compositions of late Cenozoic alkali basalts in South Korea: evidence for mixing between the two dominant asthenospheric mantle domains beneath East Asia. Chem Geol 232:134–151

Dick HJB, Bullen T (1984) Chromian spinel as a petrogenetic indicator in abyssal and alpine-type peridotites and spatially associated lavas. Contrib Mineral Petrol 86:54–76

Downes H (2001) Formation and modification of the shallow sub-continental lithospheric mantle: a review of geochemical evidence from ultramafic xenolith suites and tectonically emplaced ultramafic massifs of western and central Europe. J Petrol 42:233–250

Downes H, Bodinier J-L, Thirlwall MF, Lorand J-P, Fabries J (1991) REE and Sr–Nd isotope geochemistry of Eastern Pyrenean peridotite massifs: sub-continental lithospheric mantle modified by continental magmatism. J Petrol Spec Lherz Issue, pp 97–115

Draper G, Guierrez G, Lewis JF (1996) Thrust emplacement of the Hispaniola peridotite belt: orogenic expression of the mid-Cretaceous Caribbean arc polarity reversal? Geology 24:1143–1146

Duncan RA, Hargraves RB (1984) Plate tectonic evolution of the Caribbean in the mantle reference frame. In: Bonini WE, Hargraves RB, Shagam R (eds) The Caribbean–South American Plate Boundary and Regional Tectonics. Geol Soc Am Mem 162:81–93

Frey FA, Suen CJ, Stockman HW (1985) The Ronda high temperature peridotite: geochemistry and petrogenesis. Geochim Cosmochim Acta 49:2469–2491

Gaetani GA, Grove TL (1998) The influence of water on melting of mantle peridotite. Contrib Mineral Petro 131:323–346

Giunta G, Beccaluva L, Coltorti M, Siena F, Vaccaro C (2002) The southern margin of the Caribbean Plate in Venezuela: tectono-magmatic setting of the ophiolitic units and kinematic evolution. Lithos 63:19–40

Green TH, Blundy JD, Adam J, Yaxley GM (2000) SIMS determination of trace element partition coefficients between garnet, clinopyroxene and hydrous basaltic liquids at 2–7.5 GPa and 1080–1200°C. Lithos 53:165–187

Grégoire M, McInnes BIA, O'Reilly SY (2001) Hydrous metasomatism of oceanic sub-arc mantle, Lihir, Papua New Guinea Part 2. Trace element characteristics of slab-derived fluids. Lithos 59:91–108

Griffin WL, O'Reilly SY, Ryan CG (1999) The composition and origin of sub-continental lithospheric mantle. In: Fei Y, Bertka M, Mysen BO (eds) Mantle petrology; field observation and high pressure experimentation—a tribute to Francis R. (Joe) Boyd. Geochem Soc Spec Publ Vol 6, pp 13–45

Grover GM, Lindsley DH, Bence AE (1980) Experimental phase relations of olivine vitrophyres from breccia 14321: The temperature- and pressure-dependence of Fe–Mg partitioning for olivine and liquid in a highlands melt-rocks. In: Proc Lunar Planet Sci Conf 11th, pp 179–196

Hannah RS, Vogel TA, Patino LC, Alvarado GE, Perez W, Smith DR (2002) Origin of silicic volcanic rocks in Central Costa Rica: a study of a chemically variable ash-flow sheet in the Tiribi Tuff. Bull. Volcan 64:117–133

Hanan BB, Blichert-Toft J, Pyle DG, Christie DM (2004) Contrasting origins of the upper mantle revealed by hafnium and lead isotopes from the Southeast Indian Ridge. Nature 432:91–94

Hanson GN, Langmuir CH (1978) Modelling of major elements in mantle-melt systems using trace element approaches. Geochim Cosmochim Acta 42:725–741

Hart SR (1984) A large-scale isotope anomaly in the southern hemisphere mantle. Nature 309:753–757

Hartmann G, Wedepohl KH (1990) Metasomatically altered peridotite xenoliths from the Hessian Depression (Northwest Germany). Geochim Cosmochim Acta 54:71–86

Hartmann G, Wedepohl KH (1993) The composition of peridotite tectonics from the Ivrea Complex, northern Italy: residues from melt extraction. Geochim Cosmochim Acta 57:1761-1782

Hauri EH, Wagner TP, Grove TL (1994) Experimental and natural partitioning of Th, U, Pb and other trace elements between garnet, clinopyroxene and basaltic melts. Chem Geol 117:149–166

Hutchison R (1974) The formation of the earth. Nature 250:556–558

Ionov DA, Bodinier J-L, Mukasa SB, Zanetti A (2002) Mechanism and sources of mantle metasomatism: major and trace element compositions of peridotite xenoliths from Spitsbergen in the context of numerical modeling. J Petrol 43:2219–2259

Jagoutz E, Palme H, Baddenhausen H, Blum K, Cendales M, Dreibus G, Spettel B, Lorenz V, Wänke H (1979) The abundances of major, minor and trace elements in the earth's mantle as derived from primitive ultramafic nodules. In: Proc Lunar Planet Sci Conf 10th, pp 2031–2050

Jochum KP, Verma SP (1996) Extreme enrichment of Sb, Tl and other trace elements in altered MORB. Chem Geol 130:289–299

Johnson KTM, Dick HJB, Shimizu N (1990) Melting in the oceanic upper mantle: an ion microprobe study of diopsides in abyssal peridotites. J Geophys Res 95:2661–2678

Kennedy AK, Lofgren GE, Wasserburg GJ (1993) An experimental study of trace element partitioning between olivine, orthopyroxene and melt in chondrules: equilibrium values and kinetic effects. Earth Planet Sci Lett 115:177–195

Kerr AC, Iturralde-Vinent MA, Saunders AD, Babbs TL, Tarney J (1999) A new plate tectonic model of the Caribbean: Implications from a geochemical reconnaissance of Cuban Mesozoic volcanic rocks. GSA Bull 111:1581–1599

Kogiso T, Tatsumi Y, Nakano S (1997) Trace element transport during dehydration processes in the subducted oceanic crust: 1. Experiments and implications for the origin of ocean island basalts. Earth Planet Sci Lett 148:193–205

Kopylova MG, Caro G (2004) Mantle xenoliths from the Southeastern Slave Craton: evidence for chemical zonation in a thick, cold lithosphere. J Petrol 45:1045–1067

Kopylova MG, Russell JK (2000) Chemical stratification of cratonic lithosphere: constraints from the Northern Slave craton, Canada. Earth Planet Sci Lett 181:71–87

Maalϕe A, Aoki K (1977) The major element composition of the upper mantle estimated from the composition of lherzolites. Contrib Mineral Petrol 63:161–173

MacKenzie DB (1960) High-temperature alpine-type peridotite from Venezuela. Geol Soc Am Bull 71:303–318

Mattson PH (1985) Ultramafic and gabbroic rocks of Venezuela as possible ophiolites: Tinaquillo peridotite complex. Cuarto Congr Geol Venz Mem (Trans) 4:2514–2539

McCulloch MT, Gamble JA (1991) Geochemical and geodynamical constraints on subduction zone magmatism. Earth Planet Sci Lett 102:358–374

McDonough WF (1990) Constraints on the composition of the continental lithospheric mantle. Earth Planet Sci Lett 101:1–18

Mukasa SB, Shervais JW (1999) Growth of subcontinental lithosphere: evidence from repeated dike injections in the Balmuccia lherzolite massif, Italian Alps. Lithos 48:287–316

Mukasa SB, Shervais JW, Wilshire HG, Nielson JE (1991) Intrinsic Nd, Pb, and Sr isotopic heterogeneities exhibited by the Lherz Alpine peridotite massif, French Pyrenees. J Petrol Spec Lherz Issue, pp 117–134

Münker C, Weyer S, Scherer E, Mezger K (2001) Separation of high field strength elements (Nb, Ta, Zr, Hf) and Lu from rock samples for MC-ICPMS measurements. Geochem Geophys Geosyst 2: DOI: 10/1029:2001GC000183

Norcross C, Davis DW, Spooner ETC, Rust R (2000) U–Pb and Pb–Pb age constraints on Paleoproterozoic magmatism, deformation and gold mineralization in the Omai area, Guyana Shield. Precam Res 102:69–86

Ostos M, Avé Lallemant HG, Sisson VB (2005) The alpine-type Tinaquillo peridotite complex, Venezuela: fragment of a Jurassic rift zone? In: Avé Lallemant HG, Sisson VB (eds) Caribbean–South American plate interactions, Venezuela. Geol Soc Am Spec Paper 394, pp 207–222

Ostos M, Sisson VB (2005) Geochemistry and tectonic setting of igneous and metaigneous rocks of northern Venezuela. Geol Soc Am Spec Paper 394, pp 119–156

Palme H, Nickel KG (1985) Ca/Al ratio and compositions of the Earth's upper mantle. Geochim Cosmochim Acta 49:2123–2132

Pearson DG, Davies GR, Nixon PH (1993) Geochemical constraints on the petrogenesis of diamond facies pyroxenites from the Beni Bousera peridotite massif, North Morocco. J Petrol 34:125–172

Pearson DG, Nowell GM (2003) Dating mantle differentiation: a comparison of the Lu–Hf, Re–Os and Sm–Nd isotope systems in the Beni Bousera peridotite massif and constraints on the Nd–Hf composition of the lithospheric mantle. Geophys Res Abstracts 5:05430

Pearson DG, Nowell GM (2004) Re–Os and Lu–Hf isotope constraints on the origin and age of pyroxenites from the Beni Bousera peridotite massif: implications for mixed peridotite-pyroxenite mantle sources. J Petrol 45: 439–455

Pindell J, Kennan L, Maresch WV, Stanek K-P, Draper G, Higgs R (2005) Plate-kinematics and crustal dynamics of circum-Caribbean arc-continent interactions: tectonic controls on basin development in Proto-Caribbean margins. Geol Soc Am Spec Paper 394:7–52

Pindell JL (1993) Regional synopsis of Gulf of Mexico and Caribbean evolution. In: Pindell JL, Perkins BF (eds) Mesozoic and early Cenozoic development of the Gulf of Mexico and Caribbean region: A context for hydrocarbon exploration. Gulf Coast Section, SEPM Foundation 13th Annual Research Conference, Houston, pp 251–274

Pindell JL, Cande SC, Pitman III WC, Rowley DB, Dewey JF, Labrecque J, Haxby W (1988) A plate-kinematic framework for models of Caribbean evolution. Tectonophysics 155:121–138

Rampone E, Hofmann AW, Piccardo GB, Vannucci R, Bottazzi P, Ottolini L (1996) Trace element and isotope geochemistry of depleted peridotites from an N-MORB type ophiolite (Internal Liguride, N. Italy). Contrib Mineral Petrol 123:61–76

Rampone E, Hofmann AW, Piccardo GB, Vannucci R, Bottazzi P, Ottolini L (1995) Petrology, mineral and isotope geochemistry of the External Liguride peridotites (Northern Apennines, Italy). J Petrol 36:81–105

Reisberg L, Allègre CJ, Luck J-M (1991) The Re–Os systematics of the Ronda ultramafic complex of southern Spain. Earth Planet Sci Lett 105:196–213

Reisberg L, Zindler A (1986) Extreme isotopic variation in the upper mantle: evidence from Ronda. Earth Planet Sci Lett 81:29–45

Reisberg L, Zindler A, Jagoutz E (1989) Further Sr and Nd isotopic results from peridotites of the Ronda ultramafic complex. Earth Planet Sci Lett 96:161–180

Ringwood AE (1979) Origin of the Earth and Moon. Springer, Berlin Heidelberg New York, pp 295

Salters (1996) The generation of mid-ocean ridge basalts from the Hf and Nd isotope perspective. Earth Planet Sci Lett 141:109–123

Salters VJM, White WM (1998) Hf isotope constraint on mantle evolution. Chem Geol 145:447–460

Salters VJM, Zindler A (1995) Extreme $^{176}Hf/^{177}Hf$ in the suboceanic mantle. Earth Planet Sci Lett 129:13–30

Scherer E, Münker C, Mezger K (2001) Calibration of the Lutetium–Hafnium clock. Science 293:683–687

Seyler M, Mattson PH (1989) Petrology and thermal evolution of the Tinaquillo peridotite (Venezuela). J Geophys Res 94:7629–7660

Seyler M, Mattson PH (1993) Gabbroic and pyroxenite layers in the Tinaquillo, Venezuela, peridotite: succession of melt intrusions in a rising mantle diaper. J Geol 101:501–511

Seyler M, Paquette J-L, Ceuleneer G, Kienast J-R, Loubet M (1998) Magmatic underplating, metamorphic evolution and ductile shearing in a Mesozoic lower crustal–upper mantle unit (Tinaquillo, Venezuela) of the Caribbean belt. J Geol 106:35–58

Sinton CW, Duncan RA, Storey M, Lewis J, Estrada JJ (1998) An oceanic flood basalt province within the Caribbean plate. Earth Planet Sci Lett 155:221–235

Smith CA, Sisson VB, Avé Lallemant HG, Copeland P (1999) Two contrasting pressure–temperature–time paths in the Villa de Cura blueschist belt, Venezuela: possible evidence for Late Cretaceous initiation of subduction in the Caribbean. GSA Bull 111:831–848

Sneeringer M, Hart SR, Shimizu N (1984) Strontium and samarium diffusion in diopside. Geochim Cosmochim Acta 48:1589–1608

Stern RJ, Bloomer SH (1992) Subduction zone infancy: examples from the Eocene Izu–Bonin–Mariana and Jurassic California arcs. Geol Soc Am Bull 104:1621–1636

Sun S-S, McDonough WF (1989) Chemical and isotopic systematics of oceanic basalts: implications for mantle composition and processes. Geol Soc Lond Spec Publ 42:313–345

Takazawa E, Frey FA, Shimizu N, Obata M (2000) Whole rock compositional variations in an upper mantle peridotite (Horoman, Hokkaido, Japan): are they consistent with a partial melting process? Geochim Cosmochim Acta 64: 695–716

Tatsumi Y, Kogiso T (1997) Trace element transport during dehydration processes in the subducted oceanic crust: 2. Origin of chemical and physical characteristics in arc magmatism. Earth Planet Sci Lett 148:207–221

Teixeira W, Tassinari CCG, Cordani UG, Kawashita K (1989) A review of the geochronology of the Amazonian craton: Tectonic implications. Precam Res 42:213–227

Toramaru A, Fujii N (1986) Connectivity of melt phase in a partially molten peridotite. J Geophys Res 91:9239–9252

Vervoort JD, Blichert-Toft J (1999) Evolution of the depleted mantle: Hf isotope evidence from juvenile rocks through time. Geochim Cosmochim Acta 63:533–556

Vervoort JD, Patchett PJ, Gehrels GE, Nutman AP (1996) Constraints on early Earth differentiation from hafnium and neodymium isotopes. Nature 379:624–627

Voicu G, Bardoux M, Stevenson R (2001) Lithostratigraphy, geochronology and gold metallogeny in the northern Guiana Shield, South America: a review. Ore Geol Rev 18:211–236

Wänke H (1981) Constitution of terrestrial planets. Phil Trans Roy Soc Lond A303:287–302

White RV, Tarney J, Kerr AC, Saunders AD, Kempton PD, Pringle MS, Klaver GT (1999) Modification of an oceanic plateau, Aruba, Dutch Caribbean: implications for the generation of continental crust. Lithos 46:43–68

Woodhead JD, Hergt JM, Davidson JP, Eggins SM (2001) Hafnium isotope evidence for 'conservative' element mobility during subduction zone processes. Earth Planet Sci Lett 192:331–346

Yaxley GM, Green DH, Kamenetsky V (1998) Carbonatite metasomatism in the southeastern Australian lithosphere. J Petrol 39:1917–1930

Zindler A, Hart S (1986) Chemical geodynamics. Annu Rev Earth Planet Sci 14:493–571